2016

Computation Aided Design Of Multicomponent Refractory Alloys With A Focus On Mechanical Properties

Paul Daniel Clark
University of Mississippi

COMPUTATION AIDED DESIGN OF MULTICOMPONENT REFRACTORY ALLOYS WITH A FOCUS ON MECHANICAL PROPERTIES

A Thesis
Presented in partial fulfillment of requirements
For the degree of Master of Science
In the Department of Mechanical Engineering
The University of Mississippi

By
Daniel Clark
August 2016

ABSTRACT

Quantum mechanical calculations paired with exponential growth in computer processing speed has created a paradigm shift in materials discovery. Simulations can be carried out to accurately predict structure-composition-property relationships of novel systems. This work focuses on calculating elastic properties of high entropy alloys, a new class of alloys that are built from 4+ elements in equi-atomic proportion. These alloys often exhibit simple microstructures and each constituent element contributes its properties to the overall bulk properties of the amalgamated material. This "cocktail" effect has led to the discovery of many alloys which could drive technical advances in the future. Elastic properties of a solid are important because they relate to various fundamental solid-state properties and are thermodynamically linked to the specific heat, thermal expansion, Debye temperature, and melting point. The refractory based system, MoNbTaW, studied in this research, was found to have a Young's modulus of approximately 300 GPa. The elastic modulus decreased with addition of titanium over 11- 33 atomic percent. The elastic modulus however, was unchanged when adding vanadium at 11%, but saw a decrease in the range of 20% to 25%. The calculations also helped in predicting alloy compositions in which a single-phase solid solution exists, which is vital for capturing the cocktail effect of these alloys.

Keywords: High Entropy, Alloy, Elastic Properties, Density Functional Theory

LIST OF ABBREVIATIONS

DFT	Density Functional Theory
HEA	High Entropy Alloy
GPa	Giga Pascal
MPa	Mega Pascal
FCC	Face Centered Cubic
BCC	Body Centered Cubic
Å	Angstrom
K	Kelvin
kJ	Kilojoule
meV	Milli-electron volt

ACKNOWLEDGEMENTS

First, I would like to express my sincere gratitude to my advisers Dr. Amrita Mishra and Dr. Gautam Priyadarshan for introducing me to this research and for their guidance throughout graduate school. Their support, encouragement, and insight made the completion of this thesis possible. Next, I would like to thank Dr. Josh Gladden and Dr. Tejas Pandya for serving on my defense committee. I learned much from the courses they taught and appreciated the time outside of class they made for physics/CAD discussion. I would also like to thank Matt Nelms who gave valuable suggestions to the methodology of the simulations.

Finally, I would like to thank Dr. Jim Chambers who was my original adviser and cemented my decision to attend graduate school at Ole Miss. Dr. Chambers always made time to help. It didn't matter if it was his class, another class, administrative problems, or issues not even regarding school. I'll never forget his desire to pass on knowledge and his practical approach to teaching.

Some of the calculations reported in this work were carried out on equipment funded by the U.S. Army Research Office under a cooperative agreement award contract No. W911NF-11-2-0043 and the U.S. Army Engineering Research and Development Center's Military Engineering Basic/Applied "MMFP" Research Program.

TABLE OF **CONTENTS**

TABLE OF TABLES

TABLE OF FIGURES

CHAPTER 1

INTRODUCTION

1.1 History of Alloys

An alloy is a material that is a mixture of a metal and other chemical elements. The elements added to the metal can be metal themselves or a nonmetal and different quantities generally yield different material properties. The first alloy discovered was bronze around 3500 BC by the Sumerians [67]. It is widely believed that the discovery stemmed from the use of rocks used around fires. In Mesopotamia, copper ore was abundant and often had traces of tin. When these rocks were placed in a fire, smelting produced bronze. This new material was found to be stronger and more chemically resistive than copper alone and thus, bronze was crafted into tools and weapons. Bronze was so significant that an entire period of time was named in its honor. The Bronze Age, which lasted until 600BC in Europe, was soon replaced by the Iron Age. Ancient civilizations thrived as iron not only enabled better tools and weapons, but structures and transportation as well. However, soon civilizations discovered it was possible to strengthen iron by hammering it over fires. Of course, it has been known for some time now that steel is created as carbon atoms are infused in iron. Historians don't agree exactly when carbon steel was discovered, but steel was found in Asia Minor that dated to 1200BC [68]. If this creation was intentional is debatable. In the 19th century, it was well understood the carbon acting as interstitials strengthened pure iron and that various concentrations of carbon would affect the performance. Bessemer revolutionized the steel industry in 1856 by introducing the first mass production steel

facility, which operated by blowing air through molten pig iron. Today, precise percentages of carbon can be added to iron to provide the necessary properties. Further improvement of steel can be attributed to Harry Brearly who worked as a child in his father's steelwork plant [69]. As he built up his resume, firearm manufacturers took notice and requested consultation. Prior to WWI, manufacturing of firearms was increased significantly, but the high temperatures upon firing would erode the inside of the gun barrels. Brearly was tasked with finding a steel which would hold up to the heat of firing. Chromium was known to raise the melting temperature of metals and Brearly began to investigate its use in steel. After successfully alloying chromium and steel, it was standard procedure to investigate microstructures of experimental alloys by polishing and etching. Nitric acid was used for carbon steels to accomplish the etching. However, when Brearly introduced the acid to the carbon steel with chromium, it did not corrode as normal steel would. As a result, stainless steel was conceived and began to see use in kitchenware, surgical instruments, distilling devices and any other environment where corrosion could be a concern. Note that in all of the above examples that the materials were first discovered and uses were subsequently found. Accidental discovery leading to unintended utility has been a common theme throughout material science history. The holy grail of material science would be the inverse of this traditional process; being able to tailor a material to specialized applications.

In the past, alloys were predominately one element with additional elements added in small concentration (< 5 atomic percent). This was done to limit the formation of complex phases and intermetallic compounds which almost always lead to less than favorable properties. Modern material science, however, has somewhat abandoned this model and has found new classes of materials that not only suppress complex microstructures, but offer exceptional mechanical properties. One example is TRIP/TWIP steels that contain 15-30 wt. % Mn with small additions

of Al and Si [70]. These steels are lighter in weight and exhibit both large elongations (60-95%) and high flow stress (600-1100 MPa). Another example is a novel Ti alloy incorporating both Mo and W at concentrations greater than 5 at. % [71]. High entropy alloys are another class of materials that have had much discussion in the last decade. First coined in 2002, publications specifically mentioning HEAs have seen exponential growth over the last several years.

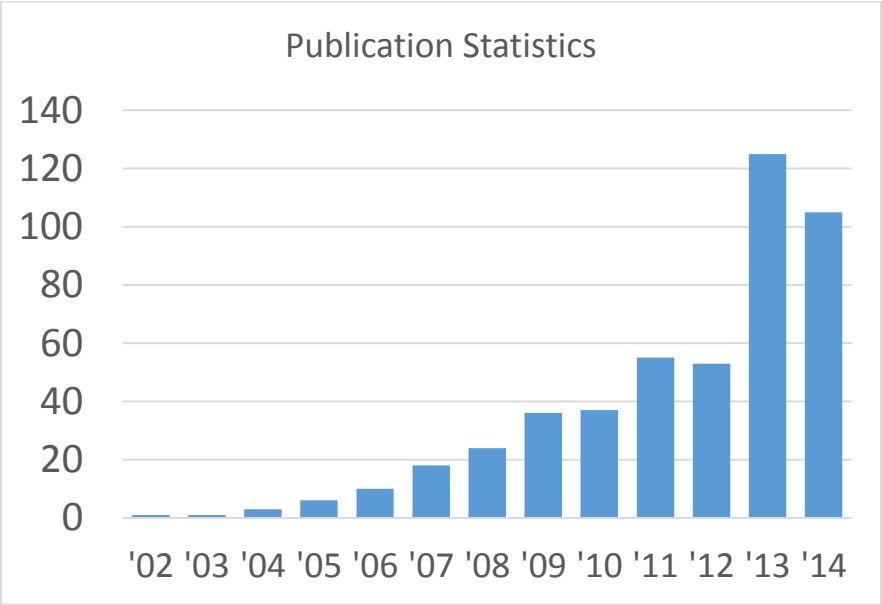

Figure 1: Publication statistics specifically mentioning HEAs [72]

1.2 Overview of HEAs

High entropy alloys (HEA) differ from conventional alloys in that the system consists of 4 to 13 elements, each represented in near equal atomic proportion. Publications exploring the properties of multicomponent alloys in near equal proportions began with Vincent [1] in 1981. As has been shown in numerous studies, multicomponent systems often have desirable properties that are not found conventional alloys. In 2014, Youssef [4] and a team of researchers discovered an alloy, $Al_{20}Li_{20}Mg_{10}Sc_{20}Ti_{30,}$ which exceeds titanium in tensile strength, yet is less dense than aluminum. Other materials, such as AlxFeCoCrNi, have unchanged expansion in wide

temperature ranges [5]. The potential applications of HEAs are limitless; automotive, aerospace, naval and energy industries could all benefit from advances in this technology.

Much information is known of systems that are based on one or two elements, but materials with three or more constituents are not very well understood as pointed out by Cantor [10]. The center of ternary phase diagrams is relatively unknown and virtually no data is available for systems that contain four elements. The figure below highlights areas in which data is known for both ternary and quaternary systems (green). White space indicates little is known and corresponds to the presence of multiple elements. Obviously, HEAs would fall in the white region as elements are represented similarly.

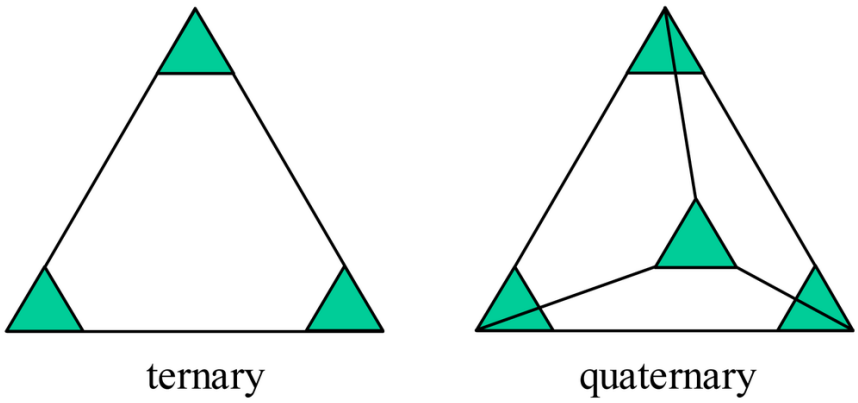

Figure 2: Areas of phase diagram which are known (green) and unknown (white) [10]

1.3 Paradigm Shift in Material Design

Cantor [2] estimates that there are approximately 10^{177} distinct alloys with the potential to be fabricated in a lab or industrial setting. This number is calculated assuming 60 of the 118

elements of the periodic table are viable options and that an alloy is distinct if a single component varies by 1%. He goes on to state that only 10^{11} alloys have been modeled or studied. This is most likely an overestimation as it is assumed that all the binary and ternary systems (again varying one component by 1% is considered a new alloy) have been studied. Therefore, a huge number of alloys, on the order of 10^{168}, have yet to be studied. To put that number into perspective, consider that there are an estimated 10^{80} stars in the universe. Obviously, the majority of these alloys will not have favorable properties or be able to outperform proven alloys. However, Cantor et al. predicts that 10^{102} systems will exhibit a single phase microstructure using the following equation:

$$N = 60(y/.1)^{60-1} = 10^{102}$$

In the formula, y is the average solubility limit that Cantor defines as 5. A single phase is sought after because it implies compatibly between all the constituent elements and eliminates intermetallic phases, which are usually brittle and can show drastically different properties within each phase. Probability suggests that many of these single-phase alloys will have properties that could unlock new applications or more effectively replace current materials in applications that have been around with little change. The question then becomes, how do scientists determine the properties of all these theoretical alloys?

There are two distinct approaches when it comes to problem solving – the Edison approach and the Tesla approach. Edison's method can best be summarized using his own words. He said, "Genius is one percent inspiration and ninety-nine percent perspiration". According to him, emphasis is placed on hard work, rather than brainstorming and systemically fine-tuning the idea based on science. Edison also said "I have not failed 700 times. I have not failed once. I have succeeded in proving that those 700 ways will not work. When I have eliminated the ways that will not work, I will find the way that will work." Here, Edison is justifying failure by claiming

that eventually something has to work. In other words, he utilized a brute-force method by trying every possible path to the solution. Tesla, however, wanted to understand the problem at a fundamental level before getting hands on. Tesla said, "I am credited with being one of the hardest workers, and perhaps I am, if thought is the equivalent of labor, for I have devoted to it almost all of my waking hours. But if work is interpreted to be a definite performance in a specified time according to a rigid rule, then I may be the worst of idlers". Traditionally, material design didn't strictly follow either of the methods, but rather accidental discovery, as was detailed previously. Over time, methods started leaning towards the Edison approach. Steel is a good example. While the discovery may have been by accident, fine-tuning to a specific application was achieved by altering carbon content until the properties were ideal. Today, steel is widely used and the properties of various compositions and heat treatments are known. The Edison approach had to be utilized in order to fill property databases, so the method, while perhaps not efficient, should not be considered poor.

Most of the papers that have been published regarding HEAs focus on fabricating materials of varying composition in hopes of stumbling upon a material that can be used in unspecified applications. This is not strictly an Edison approach as the constituent elements are chosen to maximize solubility and contribute individual properties to the alloy. This hybrid approach, in principal, sounds appealing, but it does have some negatives. Specifically, this approach will be time consuming and expensive. Fortunately, technology has improved exponentially over the years, enabling researchers to utilize computers in the search for new alloys. Additionally, functionals and potentials used to solve energy levels of alloy systems have been greatly refined and allow for accurate property and geometry calculations of systems. Ultimately, when an application presents itself and requires a material that differs from what is currently available, a

materials scientist would like to be able to first, determine the specific properties of interest. Second, pick elements that will form solid solutions with simple crystal structures and meet the required specifications. Insuring the elements will form simple phases is still a bit challenging, but improvements have been made recently that can be used as a reliable guideline. Third, use computers to ensure that the properties are as expected. Finally, fabricate the material and perform the proper heat treatment. Heat treatment is extremely important and can actually be a determining factor in whether intermetallic phases will exist.

In 2011, President Obama launched the Materials Genome Initiative, which is a collaborative network of researchers, businessmen and politicians with the goal of reducing the time it takes to bring new materials to market (often 20-30 years). This is closely related to the inverse design process outlined above. After defining the desired properties, high-throughput screening is done on the initial selection of materials, which can be on the order of 10^3-10^6. Afterwards, targeted synthesis or computational characterization is performed and a novel material with tailored properties is produced.

1.4 Motivation of Research

Computer aided pursuit of novel materials and properties will continue to increase in the coming years. The primary purpose of this research is to investigate the reliability of commercial ab-initio code, specifically in calculating theoretical elastic properties of high entropy alloys. These 21st century alloys have proven to be an important area of research due their unexpected structure and promising properties. Elastic properties, such as Young's modulus, are an atomic level property that are dependent on the bonding between atoms and not on the microstructure of the material. As a result, a simulation performed on a small number of atoms should be representative of the material at any chosen point as long as the material is isotropic. If a high

entropy alloy is carefully configured, a single phase, isotropic material should be present. Ultimately, a computer will provide data on materials that have never been fabricated in the real world.

CHAPTER 2

BACKGROUND

2.1 Overview

The name "high entropy alloy" was coined in 2004, but a strict definition has yet to be agreed upon by researchers [4]. Yeh et al. originally used the term to refer to a system of at least five metallic elements each falling within a range of 5 to 35 atomic percent. Due to this compositional requirement, it is common to see the terms "equimolar", "equiatomic" and "multicomponent" used synonymously with HEAs. Many researchers have strayed from this definition, using the term HEA to describe systems with only 4 elements or in systems in which there are 3 primary elements and 2 alloying elements that fall short of the 5% representation. The benefit of having 5+ elements in an alloy is that the configurational entropy term in the Gibbs free energy equation is minimized which leads to suppression of intermetallic phases and formation of a solid solution exhibiting a simple crystal structure. Vincent [1] published the first detailed analysis of multicomponent alloys in 1981. In 2003, Ranganthan [39] worked with similar alloys calling them multimaterial cocktails and a year later, Yeh et al. [6] coined the term high entropy alloy while studying multicomponent alloys as pointed out by Cantor [10]. Cantor goes on to state that the majority of multicomponent alloys do not exhibit high entropy and that simple phases are often present, well below the maximum limit that Gibbs phase rule gives. In addition, small changes in composition, different chemical elements and the method of fabrication will all affect the microstructure and overall properties of the material.

HEAs have drawn much attention because of their unusual, favorable properties. Some of these properties include high temperature resistance [15], high hardness [83] [84] [36], high saturation magnetization [29], high fracture toughness [85], irradiation resistance [96] and outstanding tensile ductility at both room and cryogenic temperatures [86] [87]. These properties give hope to the use of HEAs in structural applications, but the excellent wear resistance and high temperature performance has also led researchers to investigate HEA use in thin films and coatings for various applications [21] [22]. Specific compositions of HEAs have also been shown to work as diffusion barriers; preventing copper metallization in one particular case [88].

Yeh detailed four core effects for HEAs, which include: high entropy effects, sluggish diffusion, severe lattice distortion and cocktail effects [8]. High entropy effects stem from equimolar concentration of the constituent atoms, which give the alloy a high mixing entropy. This high entropy lowers the free energy of the system and encourages the formation of a single phase. Higher activation energies, resulting from atomic traps and blocks, cause sluggish diffusion in HEAs [24]. Yeh measured diffusion parameters of Co, Cr, Fe, Mn and Ni in ideal solution-like alloys by the diffusion couple method. The results were compared with diffusion parameters in various face centered cubic metals. Yeh reported that the diffusion coefficients that were measured were lower than the referenced values. In addition, Yeh found that the activation energy increases with increasing elements. Severe lattice distortion is easily explained since different sized atoms can position themselves at random lattice points. This distortion helps explain the high strength of BCC HEAs, but not low strength of single phase FCC HEAs [8].

Huhn et al. [37] pointed out two properties of high entropy alloys that warrant research in the field: cocktail effects and simple lattice stability at elevated temperatures. Cocktail effects were discussed by Yeh [8] as one of the four core effects of multicomponent alloys. The

importance of this effect is that each individual constituent will ultimately confer its properties to the overall behavior of the system. Like the philosopher's stone to alchemy, the ability to tailor a material to a specific application is a paradigm shift in material design. In the past, materials such as copper, stainless steel and vulcanized rubber were discovered unintentionally and uses were found at a later time. Coupled with today's processing power and accurate potentials, properties can be optimized using computers by varying compositions slightly. Simple lattice stability, the second important property, is crucial for carrying out these calculations. High entropy alloys often exhibit simple BCC or FCC structures rather than complex intermetallic phases which would be difficult to accurately model. Even in cases where multiple phase regions exist, the phases themselves tend toward simple Im3m or Pm3m space groups [8]. Simple phases are not only important for calculations, but complex phases often correlate to brittleness and other suboptimal properties.

There are two primary configurations of HEAs seen in publications; those based on Cr, Co, Ni and Fe and those based on Mo, Nb and Ta. After one or two additional elements are added to the matrix, the first group tends to stabilize in a FCC crystal, while the second group forms BCC lattices. Mn and Cu are the two most common elements added to Cr, Co, Ni and Fe to create FCC HEAs [5] [26] [27] [28] [34] [38] [48]. CrMnFeCoNi was discovered to be the first true single phase HEA by Cantor in 2004 [2]. In 2015, Laurent-Brocq et al. used atom probe tomography to show this solid solution on the atomic scale [66]. In addition, a phase diagram was calculated for this alloy. It was seen that a slow cooling rate would lead to a dendritic microstructure, but would become a true solid solution by annealing the dendritic structure (1100 C for 1 hour) or by increasing the rate of cooling.

Structural and mechanical properties of HEAs based on refractory metals have been a popular configuration for many researchers due to their high melting temperatures [14] [15]. Metallic alloys used in waste incinerators, turbines and space applications are currently limited to operating temperatures of around 1350C; the upper stability limit of many NiAl super alloys. However, solely using refractory metals carries the downside of high density. Therefore, additional elements such as Hf, Zr, Cr and Ti were added or substituted into the alloy in order to create a more practical material [16] [43] [58] [59]. Various concentrations of Al have also been added in order to decrease weight and form oxide scales to enhance the corrosion resistance of the alloy [58] [60]. Combinations of the aforementioned elements are of relative atomic size and the enthalpies of formation of the binaries are similar which generally lead to a simple BCC phase often with a dendritic structure, which can be homogenized with proper annealing [58]. The refractory base elements exhibit BCC crystal structures and less ductility than most FCC elements; however, Senkov et al. [61] reported a room temperature, true strain of 2.3 for HfNbTaTiZr showing that a simple weighted average approach of base elements is not completely accurate when describing toughness and ductility. This was the first successful attempt to cold roll a BCC HEA.

Wu et al. [82] reported that dislocation strengthening by dislocation multiplication played a predominate role in ZrTiNbHf. The alloy had a tensile strength of roughly 1 GPa while maintaining 14.9% plastic elongation. Other refractory HEAs such as CrNbTiZr and CrNbTiVZr have exhibited high compressive yield strengths upwards of 1.3GPa, but have limited use due to the brittle nature at room temperatures [80] [81].

2.2 Structure

From the **Table 1**, it is apparent that the final structure of many HEAs form simple BCC and FCC phases rather than complex intermetallic phases. This is because the high entropy effect in HEAs reduces the free energy of the system [41]. Chemically ordered intermetallic compounds are therefore less competitive [40]. Also, it is important to note that the constituent elements do not necessarily have to be of the same crystal type in order for the HEA to crystallize into a solid solution with a single, simple phase. The microstructure is heavily dependent on the processing method and any heat treatment or cold working that is done after solidification. Post-solidification treatment can be the difference between a single phase and multi-phase alloy.

Table 1: Structures of as-cast HEAs and constituent elements (room temp)

HEA	Constituent Element Structure						Final Structure	Ref.
	1	2	3	4	5	6		
AlCoCrCuMnFe	FCC	HCP	BCC	FCC	BCC	BCC	FCC 2 BCC	40
AlCoCrCuMnTi	FCC	HCP	BCC	FCC	BCC	HCP	FCC 2 BCC Intermetallic ($AlCu_2Mn$)	40
HfMoTaTiZr	HCP	BCC	BCC	HCP	HCP	--	BCC (dendrite and interdendrite)	43
HfMoNbTaTiZr	HCP	BCC	BCC	BCC	HCP	HCP	BCC (dendrite and interdendrite)	43
WnbMoTa	BCC	BCC	BCC	BCC	--	--	BCC (Dendritic)	14
WnbMoTaV	BCC	BCC	BCC	BCC	BCC	--	BCC (Dendritic)	14
AlCrCuNiFeCo	FCC	BCC	FCC	FCC	BCC	HCP	FCC BCC	54

Many models have been proposed to predict which combinations of elements are most likely to form single-phase solutions. Wang et al. [40] proposed 2 new variables to aid in predicting the formation of stabilized solid solutions in HEAs. The first parameter, k_n, is a function of the number of constituent elements and the second parameter, ψ, is defined as the sum of elemental melting temperatures divided by the sum of the binary mixing enthalpies. It was theorized that if $\psi>1.1/k_n$ then high entropy would stabilize a solid solution. It was reported that $\psi>1.1/k_n$ is equivalent to $\Omega>=1.1$; a quantity that was proposed by Yang et al. [42]. The quantities ψ and k_n were found to be calculated more conveniently than the parameter Ω [40]. While working with FCC based alloy systems, Stepanov et al. used atomic radius and valence electron concentration (VEC) to determine solubility. Stepanov et al. [47] reported that the addition of V to the known single phase FCC HEA CoCrFeMnNi saw formation of an intermetallic sigma phase as the concentration of vanadium exceeded 25%. Further, it was reported that annealing the HEA resulted in an increase of the volume fraction of the sigma phase. Prediction of the formation of the sigma phase can be carried out using a combination of VEC and δr. Stepanov suggested that VEC fall in the range of 6.88 and 7.84 for formation and that δr should be larger than 3.8%. The sigma phase, as expected with intermetallics, resulted in increased hardness and loss of ductility.

Deformation can change the microstructure of HEAs and thus affect the properties. Schuh et al. showed that under high-pressure torsion, the grain size of CoCrFeMnNi decreased, yet the FCC structure remained unchanged [62]. It was also observed that isochronal annealing done after the plastic deformation lead to an increase in hardness followed by softening as the temperature was increased. Isothermal annealing done at the peak hardness yielded an even greater hardness value. Microstructural analysis performed on the HEA showed that nano-scale phases were embedded in the HEA at the grain boundaries. It was reported that longer annealing times can

increase the number of nano scale precipitates at the grain boundaries and this was the reason for the increased hardness [62]. Thus, HEAs used in high temperature environments must be carefully observed under long exposure times, as nano phases can take longer than expected to form.

While numerous studies have been published that seek to explain the deformation mechanics in HEAs, little is known due to several factors pointed out by Otto et al. [63]. First, many HEAs that are reported in publication contain intermetallic compounds which invalidates data relating to the solid solution phase. This is especially true of tensile and compressive testing. Next, even in the absence of intermetallic compounds, multiple distinct solid solution phases can be present which act together to yield a single numeric test result; if a particular region is of interest, the previously acquired data is simply an approximation. Finally, little effort has been made to refine the grain sizes in cast alloys that are truly single phase. Specifically, as-cast HEAs exhibit a dendritic microstructure upon solidification. Different concentrations of elements are usually seen between the dendritic and inter-dendritic regions of the alloy. This imbalance, as well as coarse grains leads to more complex deformation mechanics that may not be seen in a fine grain, solid solution. In addition to these shortcomings, dislocation movement in HEAs is not understood due to the random configuration of atoms in the crystal's lattice. Dislocations must somehow move through the lattice of constantly varying atoms and placement.

Table 2: Lattice parameters of HEAs

HEA	Phase	Lattice Parameter (A)	Reference
AlCoCrCuMnFe	BCC1	3.01	40
	BCC2	2.89	
	FCC	3.69	
AlCoCrCuMnTi	BCC1	2.98	40
	BCC2	3.17	
	FCC	3.58	
	$AlCu_2Mn$-like	2.97	
HfMoTaTiZr	BCC*	3.376	43
HfMoNbTaTiZr	BCC*	3.370	43
CoCrFeNiMn	BCC **	2.878	46
	FCC **	3.536	
CoCrFeMnNi (as-solidified)	FCC	3.592	47
$CoCrFeMnNiV_{.25}$ (as-solidified)	FCC	3.597	47
$CoCrFeMnNiV_{.5}$ (as-solidified)	FCC	3.606	47
	Tetragonal	a = 8.820 c = 4.569	
$CoCrfeMnNiV_{.75}$ (as-solidified)	FCC	3.607	47
	Tetragonal	a =8.822 b = 4.573	
CoCrfeMnNiV (as-solidified)	FCC	3.603	47
	Tetragonal	a = 8.827 c = 4.579	
WnbMoTa	BCC	a = 3.213	14
WnbMoTaV	BCC	a = 3.183	14

* Dendritic and interdendritic regions both exist with similar parameters

** Milling time affects data

It should be noted that the actual atomic percentages in the HEAs differed slightly from the nominal values seen in the chemical equations. The percent error was upwards of 10% in some cases which had some impact on the lattice parameters. Also, it can be shown that the use of Vegard's Law (weighted average approach) is accurate in many cases [43]. Wei et al. [46] showed that milling time affects both the crystalline size and lattice parameter when HEAs are fabricated

using mechanical alloying. Specifically, the lattice parameter of the BCC phase of the CoCrFeNiMn alloy dropped from 2.866 to 2.878 as the milling time increased from twelve hours to sixty hours.

The structure of the HEA is often the dominant factor which drives mechanical properties [3]. For example, Zhou [28] found that $AlCoCrFeNiTi_{.5}$ exhibited a BCC structure and had a yield strength of 2.26 GPa, which is larger than most high strength alloys including bulk glasses. In general, BCC-structured HEAs have been shown to have high strength and low plasticity. FCC-structured HEAs, however, have been reported to possess high plasticity and low strength [3, 27].

Experimentally, X-ray diffraction and scanning electron microscopy are used to observe the microstructure of the alloy. In the **Figure 3**, a dendritic structure can be seen in $CrMo_{.5}NbTa_{.5}TiZr$ which is common among as-solidified samples. In the 10 micron image, both BCC and a Lave intermetallic phase are present. After heat treatment (HIP) for 3 hours at 1450C, the dendrties were found to be more coarse and rounder in shape. However, annealing at 1000C for 100 hours did not change the size or morphology for the BCC1 phase. Computer simulated equilibrium phase diagram were developed using CompuTherm LLC, but were not consistent with experimental results. The Scheil simulation predicted 83% BCC1, 12% BCC2 and 5% Laves, but experiments yielded 42% BCC1, 27% BCC2 and 31% Laves.

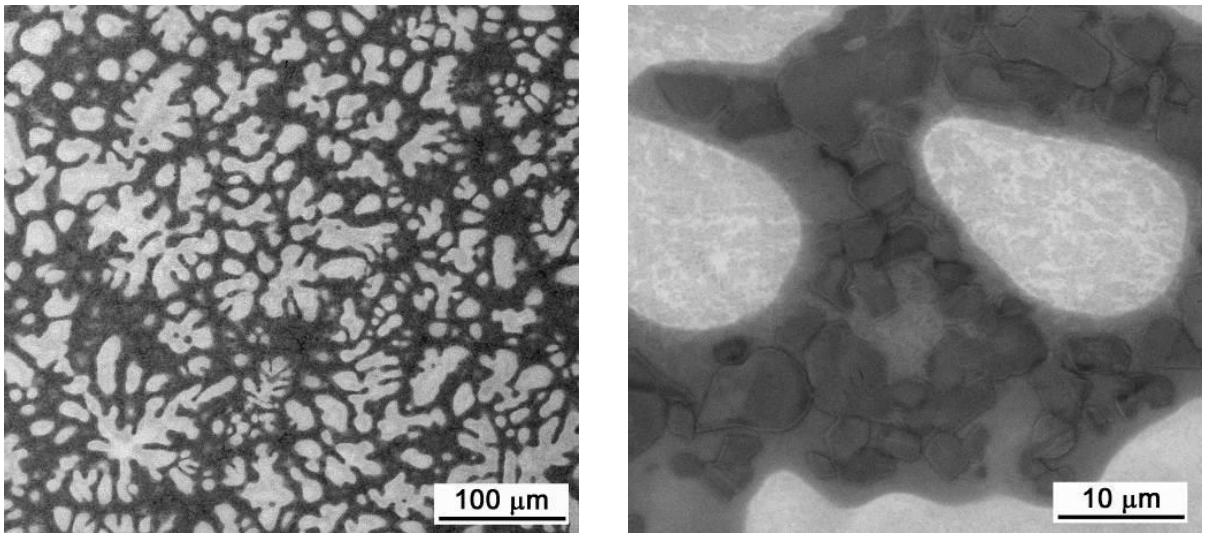

Figure 3: Dendritic structure in an as-solidified HEA [35]

2.3 Properties

2.31 Mechanical

Table 3: Mechanical properties of various HEAs

HEA	Yield Strength (Mpa)	Compressive Strength (Mpa)	Ultimate Strain (%)	Vickers Hardness	Ref
AlCoCrCuMnFe	1110.9	1529.3	15.2	447.9	40
AlCoCrCuMnTi	1568.0	1947.9	10.9	554.8	40
HfMoTaTiZr	1600	--	4 (Fracture)	542	43
HfMoNbTaTiZr	1512	--	12 (F)	505	43
CoCrFeMnNi	--	230	Not fractured	144	47
CoCrFeMnNiV	--	1660	1845 (F)	650	47
WnbMoTa	--	--	--	4455	14
WnbMoTaV	--	--	--	5250	14
$Al_{.5}$NbTiMoV	1625	--	--	--	23

A weighted average approach to property prediction should be avoided with high entropy alloys as can be seen in many studies. One notable example were tensile and compressive tests

performed by Wang et al. on a sample of $CoCrCuFeNiAl_{.5}$. A tensile strength of 707 Mpa and a plastic strain limit of 19% were reported [26] on the HEA that exhibited a face centered cubic solid solution phase. Accepted tensile strength values of Co, Cr, Cu, Fe, Ni and Al are 760, 103, 210, 350, 140 and 40 Mpa, respectively. The average value of these numbers would be significantly lower. It is known that the presence of intermetallic compounds usually increase an alloys hardness while decreasing ductility due to its brittle nature. This phenomena is also seen with HEAs and is evident when looking at the mechanical testing of two similar alloys performed by Wang et al. [40]. The first as-cast alloy, AlCoCrCuMnFe, exhibited 3 simple phases and showed ductile behavior and a Vickers hardness of 447.9. Fabrication of AlCoCrCuMnTi saw an intermetallic phase in addition to the 2 BCC and single FCC phases. Tensile testing resulted in a more brittle stress-strain curve and a hardness of 554.8.

Solid solution strengthening plays an important role in HEAs as dislocations have a difficult time maneuvering through the distorted lattice. Due to the random configuration of atoms, the line defects move through constantly changing environments. Precise knowledge of dislocation dynamics in HEAs is not known at this time, but much research is being performed both experimentally and theoretically.

Chien-Chang at el. [43] fabricated two HEAs based off of a previous refractory HEA study performed by Senkov et al. [16] in order to improve the mechanical properties for potential use in turbine technology. The study of HfNbTaTiZr conducted by Senkov et al. showed unfavorable strength at high temperatures while exhibiting plasticity of 50%+ at room temperature. HEAs based on refractory metals tend to show the opposite, i.e. exceptional high temperature strength and brittleness at room temperature. Chien-Chang et al. thus altered the composition to retain the room temperature ductility and increase the strength at high temperatures. Two HEAs were

fabricated using vacuum arc melting, HfMoTaTiZr and HfMoNbTaTiZr. Molybdenum was chosen due to a favorable Young's modulus and a melting temperature of 2623C. Hirai et al. [44] showed molybdenum improved high temperature mechanical properties in situ composites and Yeh [45] reported that hot hardness increases with increasing molybdenum concentration as pointed out by [43]. The hope was that molybdenum's properties contributed to the cocktail effect in a way such that the alloy was tailored to a specific use. It was found that both HfMoTaTiZr and HfMoNbTaTiZr maintained a BCC phase and that the high temperature properties were improved. Specifically, the addition of molybdenum to HfNbTaTiZr (in equal proportion) increased the yield strength six-fold at 1200C. As reported, the fracture strain of 12% was observed at room temperature indicating a successful contribution of molybdenum.

Nayan et al. reported a deformation activation energy value of 306 kJ/mol for AlCrCuNiFeCo. This was the first reported activation energy for a HEA and thus no data exist in which to compare [54]. In addition, Nayan et al. employed the processing map approach [56] to identify the optimum temperatures and strain rates for hot working the HEA. It was reported that the instabilities predicted from the mathematical models were confirmed by experimental procedures. Specifically, imaging of the alloy stressed at 700C showed formation of cracks which was predicted by the equations. Strain rates for optimum processing were found to be in the range of 10^{-3}-$10^{-2.5}$/s at temperatures of 800C-1000C.

At cryogenic temperatures, unexpected mechanical properties have been discovered in several HEAs. Otto et al. [62] reported that a sample of CoCrFeMNi displayed a higher ductility at 77K than at room temperature. The sample was arc melted, casted, cold-rolled and then recrystallized to homogenize the microstructure and refine the grain size. Deformation-induced twinning likely contributes to the increased ductility as well as an increase in work hardening due

to the extra interfaces that the twinning causes. However, the specific microstructural processes that arise due to change in temperature need to be studied further [62] [63].

As with traditional alloys, trace amounts of various elements can be added to HEAs to alter the properties. Several publications focus on hardening the surface of materials using methods such as flame hardening, weld hardening and various coating methods. One such example of the latter was nitriding conducted on a FeNiMnAlCr system. Meng and Baker [64] heated the alloy to allow nitrogen to diffuse into the surface. Several factors such as constituent elements in the alloy, nitriding temperature, cooling rate, and post nitriding annealing all affect the hardness of the resulting surface. It was reported that the nitrogen removed most of the Al from the matrix and formed AlN hardening the material's surface. An increase in the hardness was directly correlated to lower nitriding temperatures. The HEA before nitriding consisted of both FCC and B2 phases but exhibited a single FCC phase after the aluminum nitride was formed. It was also concluded that addition of Cr led to deeper penetration of AlN precipitation further hardening the material.

2.32 Magnetic

Exploration of magnetic properties of HEAs have been focused on materials with Fe, Co and Ni as three of the elements since high concentrations of magnetic elements lead to higher magnetization [18, 76, 77, 78, 89]. Saturation magnetization values of 10-50 emu/g have been reported; primarily derived from Al-Co-r-Fe-Ni-Ti [18]. Zhang et al. [29] reports that alloying elements, such as Cr, can greatly affect the magnetic properties of the HEA since magnetization is cancelled because of anti-parallel magnetic coupling between Cr and Fe/Co/Ni. Kourov et al. [76] showed that magnetic properties are highly temperature dependent in melt spun samples of AlCrFeCoNiCu and will undergo a change from ferromagnetic to paramagnetic when temperatures exceed 900K. Solidification can also play an important role in determining if a HEA will exhibit

magnetic anisotropy [89]. Directional solidification for example, allows for more control over the grain morphology, thus improving soft magnetic properties.

2.33 Electrical

Electrical properties including resistivity $\rho(T)$, magnetoresistance $\Delta\rho/\rho_0$ and the absolute differential thermal emf S(T) are the most commonly reported values of electrical properties. Kourov et al. [76] found an anomaly in the a plot of S(T) versus temperature plot that suggests a rearrangement of the electronic band structure in AlCrFeCoNiCu systems that fall below 50K.

2.34 Optical

Information about the electronic band structure can be found by analyzing certain optical properties, most commonly the refractive index $n(\lambda)$ and the absorption coefficient $k(\lambda)$. When looking at plots of optical conductivity, HEAs do not exhibit the maxima and minima that single elements or binary compounds will. This is because the loss of identity of any individual element and a composite, or cocktail, effect is present which smears the profile [76].

2.4 Fabrication Methods

Fabrication methods of HEAs can be classified by the starting state of the constituent elements [3]. The classifications are:

1. From solids
2. From liquids
3. From gases
4. From electrochemical processes

The most widely utilized form of solid alloy formation is mechanical alloying. The first step is to combine the elements in a ball mill which grinds them to a fine powder. The powder is then compressed and sintered by way of a hot-isostatic-pressing process. Lastly, internal stresses are removed by heat treatment. Chen et al. [31] prepared BeCoMgTi and BeCoMgTiZn from elemental powders by mechanical alloying. All of the elements used were of HCP structure, yet formed an amorphous phase after milling. It was reported that chemical incompatibility, high entropy effects and large atomic size differences prevented the formation of a solid solution.

Preparation from gases is generally used in thin-film deposition and uses a type of sputtering technique. A target is placed in a vacuum chamber along with elements that will coat the material. A voltage is applied across the chamber in order to eject atoms from the alloy to the target. Electrochemical preparation is an innovative, uncommon method for HEA production, but was used by Yao to prepare BiFeCoNiMn [32]. This method is especially useful for improving surface wear resistance of other materials as shown by Lin et al. [22]. Not only did (AlCrTaTiZr) NxSiy HEA coatings exhibit FCC solid solution coatings for multiple compositions, but, the material had a very high wear resistance with a hardness value of 30.2 GPa.

Liquid preparation is the most common method of HEA formation with arc melting being used most frequently [36] [21]. Here, elements are melted together in a furnace with torch temperatures upwards of 3000C [3]. Care must be taken to ensure that none of the elements being melted evaporate. Zn, for example, is a common metal used in HEAs, but it's relatively low melting point make arc melting a poor choice. For multicomponent alloys consisting of lower melting point elements, induction heating can be used. In this process, an electrically conducting material is heated using electromagnetic induction. This generates Eddy currents and resistance leads to Joule heating of the metal [33].

As with conventional alloys, altering the microstructure of HEAs by processing will change the properties of the material. Wang [34] prepared as-cast samples of AlCoCrFeNi in order to study the cooling rate effects on the microstructure and mechanical behavior of the alloy. It was reported that increased cooling rates lead to more uniformed microstructures and reduced inter-dendrite composition. In addition, strength and plasticity both saw marginal increases. Recently, there has been a lot of interest in examining the role of various processes in order to improve or alter the properties of HEAs. Some of these methods include: Controlled solidification [89], 23hermos-mechanical treatment [55], alloying [97] [98], annealing [99] and age hardening [100] [101].

Rate of solidification after mixing the elements greatly affect the outcome of the microstructure as well as any hot working or cold working done during processing. HEAs that are produced through melt casting usually exhibit a dendritic microstructure [49-53] which yields unfavorable properties as pointed out by Nayan et al. [54]. Elemental segregation causes the solidification of dendritic microstructures. In addition, cast alloys show chemical heterogeneity, shrinkage porosity and metastable eutectics at grain boundaries [54-55]. Much research is focused on various processes to alter the properties of these cast alloys. For example, controlling crystal orientation via directional solidification has been used to increase ductility and magnetic coercivity in many lower ordered systems. Zuo et al. [89] showed that this processing method is just as beneficial in HEAs. It was reported that the coercivity of a FeCoNiAlSi HEA was reduced and the alloy possessed magnetic anisotropy. Li et al. [94] showed that supercooling CoCrFeNi via the glass fluxing method enhanced the alloys compressive yield strength by roughly three times. This effect was attributed to grain refinement and the precipitation of a BCC phase, which has been shown to increase the strength of materials [95].

2.5 Modeling

In order to accurately model any system, the underlying physics must be known. Prediction of alloy formation requires the knowledge of all possible interactions among the constituent atoms. If atomic interaction is fully described, then everything is known about the material including properties and the phases present. Therefore, every electron-electron repulsive force and every electron-nuclear attractive force must be accounted for in a material which may have on the order of 10^{25} atoms. In addition, the kinetic energy of the atoms itself will play a role in alloy formation. Of course, approximations can be applied as nearest neighbor interactions dominate. The motion of quarks and leptons, which constitute atoms, are subject to the laws of quantum mechanics and must be applied to perform first principal, or ab initio, simulations. Nature is probabilistic and thus quantum mechanics will yield the most probable configuration, binding energy or whatever result is sought from the calculation. Different formulations of the basic quantum mechanical equations, as well as coding (i.e. numerical integration) will obviously affect the outcome of the simulation. Many software packages are open source and allow the user to customize functionals or mathematical code. Others, like the CASTEP module of Material Studio, are commercialized and do not allow access to the coding. Ab initio investigations into HEAs are rare, due in part to the recent discovery of these alloys, but also because the computational power required is still expensive and time consuming even with today's supercomputers. Work done by Tian et al. is one of the first promising looks at modeling HEAs using a first principal approach [74] [75].

There have been several studies employing DFT to study the properties and stability of intermetallic compounds [91] [92]. Zhi-sheng et al. expanded on this topic by using CASTEP to find structural, electronic and elastic data for every intermetallic compound that could form in an alloy of FeTiCoNiVCrMnCuAl [90]. This data was used to understand how intermetallic

compounds affect the properties of HEAs. It was concluded that intermetallic phases with values of formation less than -.35eV/atom and values of cohesive energy greater than -7.0eV/atom have more stable crystal structures and thus, have a higher probability of formation. As expected, elastic property calculations yielded shear modulus and elastic modulus data which showed intermetallics would increase hardness of the HEA. Li et al. [79] performed ab initio calculations on four refractory HEAs based on Zr, V, Ti, Nb and Hf using the Exact Muffin-Tin Orbitals – Coherent Potential Approximation (EMTO-CPA) and found that the theoretical data was consistent with available experimental data.

2.6 Conclusion

From published research, calculations using a weighted average approach can be used accurately in many cases to predict both the lattice parameters and the density. This is especially true if the atomic radii of the constituent elements are similar and the crystal structure is the same. In general, density and lattice parameters of systems that obey the Hume-Rothery rules can be predicted even for multicomponent alloys. Hardness is the obvious exception [14,43]. Solid solution strengthening plays a role in increasing the hardness of single phase multicomponent alloys and the weighted average approach leads to erroneous calculations. The crystal structure itself can also be predicted by analyzing the binary phase diagrams. Exceptions exist in all cases and more accurate methods are needed to fully understand the behavior of HEAs.

Zhang et al. [3] lists 9 areas which need to be studied further to obtain a fundamental understanding of HEAs. First, the sources of entropy need to be quantized. Collective excitation of particles in a periodic structure can be measured using inelastic neutron scattering and nuclear resonant inelastic X-ray scattering. This data will help quantify configurational entropy of mixing of HEAs. Ravelo et al. calculated free energy and vibrational energy differences of an ordered and

disordered Ni_3Al system [25]. Next, phase diagram information is severely lacking in systems of more than five elements. CALPHAD modeling will aide in building a thermodynamic database for such alloys. In addition, crucial values, such as Gibb's free energy and enthalpy, can be calculated directly. As reported by Yeh [8], multicomponent alloys exhibit sluggish diffusion and lattice distortion. However, these quantities cannot be accurately measured at this time. Utilization of computer modeling will again expedite the process of these calculations. Third, the enthalpy of mixing needs to be quantized as this value determines phase stability as seen in Gibbs phase rule. Deformation mechanisms in HEAs are another area that need to be explored. It is known that dislocations and twins in crystalline alloys allow for plastic deformation; and similarly STZs and TTZs in amorphous alloys. However, it is unknown what structural units in HEAs cause plastic deformation. Zhang's other four areas of future research are:

1. Micro and nano-structures of HEAs after plastic deformation.
2. Fatigue properties, specifically at high temperatures.
3. Creep performance
4. Environmental properties

CHAPTER 3

PRELIMINARY CONCEPTS

3.1 Material Science

It is important to know the ways in which a crystal can be built before running a computer simulation as crystal structure is often an input. There are 32 point groups associated with combinations of the point group symmetry operations. The operations include rotation, inversion about an axis and mirroring. Any of these operations acting on a basis must produce an identical copy of that basis. Once the unit cell (single atom, molecule, etc.) has been built, it is translated in 3 dimensions to create one of fourteen Bravais lattice. These lattices are grouped in 7 crystal systems which include monoclinic and cubic. Creating a crystal by translation may involve one of two new symmetry operations: screw axis and glide planes. Combinations of all symmetry operations lead to 230 space groups [20]. Space groups simply define all the possible crystal symmetries.

X-ray diffraction is a vital technique in experimentally examining the crystal structure of a material. When incident electromagnetic radiation of similar wavelength reaches an obstruction, the wave will bend and is detected on a lattice that differs from the lattice of the crystal itself. The lattice which it is detected is known as the reciprocal lattice and is merely an abstraction to help visualize the atomic structure. Simple equations exists that convert the reciprocal lattice to the real lattice and vice versa. In the figure below, the crystal is located in the center of an imaginary sphere, known as the Ewald Sphere. As the light wave encounters the crystal, it is diffracted and

detected at a point d* on the reciprocal lattice. D* is related to the real lattice by 1/d, hence the name reciprocal lattice. The points on the reciprocal lattice are also given by Miller indices and is simply an alternative view of the real structure.

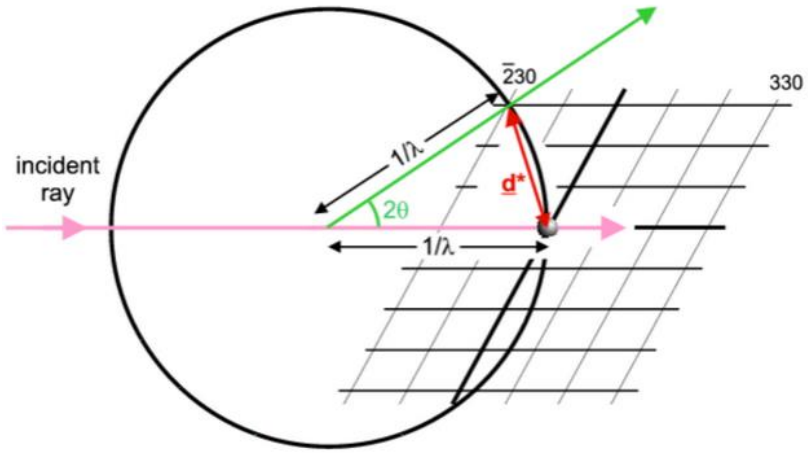

Figure 4: Reciprocal lattice [12]

The electronic band structure describes what energies the electrons in a system can have and which energy ranges are forbidden. Kinetic energy is proportional to the velocity squared as seen in the elementary equation $E_k=mv^2$. Since an electron has both wave and particle properties, the velocity can be expressed in terms of the wavenumber (wavelength per unit distance). Hence, the kinetic energy of an electron is also proportional to its wavenumber. In a vacuum, a lone electron's band structure plot would simply be a parabola of the form $y=x^2$. In a solid however, complications arise due to the attractive and repulsive properties of the electron to other charged particles. These electromagnetic forces give rise to energy gaps; the energy state that an electron cannot occupy. The periodicity of a crystal gives rise to a repeating band structure so that only one instance, called the first Brillouin Zone, of the band structure is needed.

3.2 Thermodynamics

Energy is perhaps the most important concept when discussing formation of alloys. Unfortunately, it is a rather abstract concept and there are many definitions depending on what is being defined. In elementary physics it is taught that energy is the ability to do work. This energy comes in two flavors, kinetic and potential. Kinetic energy is directly proportional to both the mass and the square of the velocity of the system. The system could be a particle or a continuum such as a ball. An increase in kinetic energy implies that the system is accelerating, thus the velocity must increase. Potential energy is directly proportional to the mass of the system and the height above some reference point (often the ground). Due to the conservation of energy, a decrease in potential energy often suggests an increase in kinetic energy. For example, a roller coaster at its peak has much potential energy stored, but low kinetic energy since the car is almost stalled. As the car reaches the bottom of the fall, the kinetic energy builds as the potential energy drops. In this case, there is simply a tradeoff between types of energies. However, it is possible that a system will decrease in energy and do some kind of work rather than simply trade energy among itself. For example, water flowing downwards through a paddlewheel will lose potential energy to both kinetic energy of the water as well as work done on the paddlewheel. The paddlewheel may in turn spin a shaft that provides electricity via a generator. While the energy of the system (water) decreases the total energy is conserved in electric potential. A third possibility is via a nuclear reaction in which mass becomes energy and vice versa. This is Einstein's mass-energy equivalence and will not be discussed.

Enthalpy is a specific type of energy that is used in material science and is useful when discussing fabrication and reactions. Summing the internal energy and the product of pressure and volume (PV) will yield enthalpy (measured in Joules). The PV term is the energy required to

displace particles and put the system into being. Internal energy is a measure of the energy within the system of interest and will change if heat is added or removed, work is done on or by the system and if matter is removed or added. Kinetic energy of the system as a whole is not represented by internal energy. If a bullet is shot from a gun for example, the kinetic energy of the individual particles are represented by the internal energy term and will increase after being shot as heat is expelled. Note that the average kinetic energy per molecule is defined as temperature. The kinetic energy of the projectile itself, however, does not play a part in the internal energy term. As high entropy alloys are modeled, a term for this quantity will be required. Changes in enthalpy are very important and give insight into the stability of systems. In nature, a system is most stable when its ground state energy is at a minimum and therefore, it is most likely to be found in this state. Changes in enthalpy when forming compounds from various pure elements is called enthalpy of formation. In both exothermic and endothermic reactions, it requires energy to break bonds and is conveniently known as bond energy. Further, as bonds are formed, energy is released. Both of these processes change the internal energy and thus the enthalpy. Extensive tables with standard enthalpy of formation data can easily be found in material science or thermodynamic textbooks. Assuming standard conditions is generally valid, however the enthalpy of formation is a function of temperature.

Entropy is an extensive thermodynamic property measured in Joules per Kelvin. Often thought of as a measure of disorder, this definition is a cause of concern and a more precise understanding is required to have a good insight of high entropy alloys. The term ‘entropy’ was first coined in the mid-19th century by Rudolf Clausius. While working with combustion systems, Clausius observed that there was a loss of functional energy and needed a way to quantify this energy that would not contribute to work done by the system. The original definition for change

in entropy was the heat of the system divided by the absolute temperature. Several years later, Boltzmann showed that the absolute temperature was simply the average kinetic energy of the system. A combination of these two statement shows that entropy can be thought of as the number of microscopic degrees of freedom of the system. Specifically, this is known as configurational entropy. The equation can be seen below.

$$\Delta S_{mix} = R\ln(N)$$

R in the equation is the universal gas constant and N represents the number of elements in the system. Therefore, high entropy alloys are named because N is higher than conventional alloys and thus the configurational entropy is of greater value. Qualitatively, entropy can be thought of as both a loss of functional energy and as a dispersion of energy (somewhat synonymous). Gibbs free energy connects the ideas of enthalpy and entropy and is an important concept when explaining the formation of phases in HEAs. The equation for Gibbs free energy is given below:

$$G = U + PV - TS = H - TS$$

Gibbs free energy is a measure of the energy that is available for work and systems in nature will ultimately try to minimize this number to be in a state of equilibrium. The entropy of the system, multiplied by an absolute temperature scaling factor, is subtracted from the total energy of the system to yield Gibbs free energy. To determine if a reaction is likely to take place, it is useful to imagine a seesaw with entropy and enthalpy occupying the ends. The figure below visually represents the connection between the two terms in the Gibbs free energy equation.

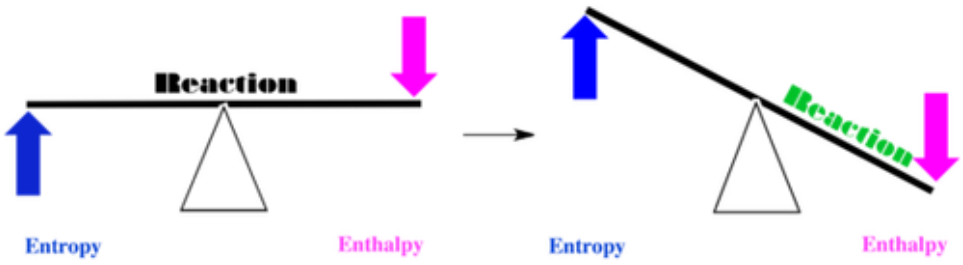

Figure 5: Favorable conditions for reaction [102]

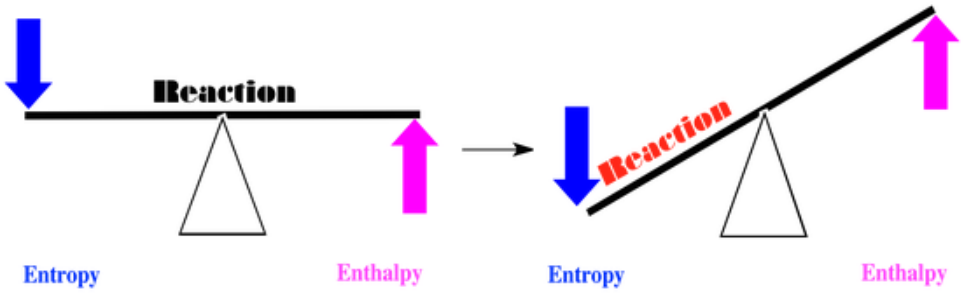

Figure 6: Unfavorable conditions for reaction [102]

In the first figure, the enthalpy wants to move from a higher to a lower energy level which encourages a reaction. Further, the entropy wants to go from a lower to a higher energy level which also encourages a reaction. In this case, the seesaw will tilt to the right and a reaction occurs which drives the system towards equilibrium. The second figure shows just the opposite and as a result the system does not react. A third case arises when both enthalpy and entropy want to proceed in the same direction. A reaction is still favorable if the decrease in enthalpy is greater than the decrease in entropy. This is consistent with the analogy as a heavier person will tilt the seesaw in his direction rather in the direction of the lighter weight person even if he is also pulling downward. In terms of HEAs, the enthalpy (specifically, the enthalpy of mixing) is a measure of the long range order of the system. When $\Delta H < 0$ formation of intermetallic compounds is usually observed. But as ΔH takes on larger positive values, phase separation is encouraged. However,

ΔS favors formation of solid solutions as the temperature scaling factor rises. Therefore, there is a competition between enthalpy and entropy with the formation of solid solutions falling somewhere near 0 Gibbs free energy. While minimizing Gibbs free energy is one way of predicting solid solution phase stability, other methods are currently being developed that look specifically at the enthalpies of formation of the individual constituents. However, these methods are still erroneous. The Hume-Rothery rules can also serve as a guideline to predicting simple phases. There are four rules of solubility for substitutional solids:

1. The solvent and solute atomic radii should differ by no more than 15%.
2. The crystal structure should be the same.
3. Valency should be equal or near equal.
4. Similar electronegativity in the constituent elements.

Broken rules usually imply that solid solutions will not form, but meeting all the criteria does not ensure solubility as exceptions always exist. Why do solid solutions tend not form if one rule is broken? If the difference in atomic radii is larger than 15%, the smaller element will generally act as an interstitial rather than occupy a lattice point in the crystal. Elements of the same crystal structure usually yield the same structure when mixed and different structures will more likely form two phases. A notable exception is mixing nickel and aluminum (both FCC) and finding the NiAl crystal to have a BCC lattice. Metals tend to dissolve in metals with higher valencies than metals with lower valencies and large differences in electronegativity result in the formation of intermetallic compounds.

Extension of these rules beyond binary systems can serve as a guideline, but difficulties arise due to the complex nature of multicomponent systems. Therefore, a more elaborate method of analysis is needed to determine if a solid solution will form in multicomponent systems. At this

time, no method exists that can predict a solid solution with 100% accuracy. In fact, only a handful of solid solution HEAs have been discovered because of the difficulties in finding a physics based approach in predicting solubility. Currently, only FCC and BCC HEAs have been discovered. CoCrFeMnNi [2] forms a solid solution HEA with a FCC crystal structure due to the same arrangement of the constituent's crystal structure. Note that the elements in this alloy have roughly the same atomic radius and are on located in the fourth period of the periodic table. The electronegativity's (1.6-1.9) and valences (all valued at 4 except chromium) are also similar, meeting all four of the substitutional solid solubility rules discussed above. The BCC HEAs found [13] consist of refractory metals and include NbMoTaW [14,15], NbMoTaVW [14,15] and HfNbTaTiZr [16]. Chen [17] attempted to form a solid solution HEA with a hexagonal closed pack crystal structure using BeCoMgTi and BeCoMgTiZn, but was not successful noting chemical incompatibility and large differences in atomic size.

Gibbs' phase rule (seen below) relates the number of components and phases associated with the system.

$$F = C - P + 2$$

C represents the number of components and P gives the maximum number of phases. The degrees of freedom, F, is the number of intensive properties the can be altered simultaneously without causing change to another. Often, the intensive properties are temperature and pressure and lead to F equaling 2. If pressure is invariant, subtraction by 1 on each side of the equation is usually given. It was discovered that multicomponent alloys usually form phases that are well below the maximum value obtained using Gibb's rule and may instead form solid solutions [2,6,7]. Yeh [8] explained this stating that high entropy effects will stabilize high entropy phases.

3.3 Density Functional Theory

Two main formulations exist which aid in describing the behavior of a dynamic system. The first is a Newtonian approach and is beneficial in such cases where systems are large. A Hamiltonian approach, or energy approach, is very useful in small systems where interactions between electrons and nuclei dominate. Density Functional Theory (DFT) is a quantum mechanical modeling technique that essentially solves the Schrodinger equation in order to explain how a system will evolve. The advantage of DFT is that it works with density as a function of position rather than the wave function, which depends on the position of every particle as well as an electron spin. The density-functional perspective is therefore quite different than the many-body perspective as illustrated in the figure below. Mathematically, DFTs parameters require $\rho(\mathbf{r})$ rather than $\Psi(\mathbf{x_1},\mathbf{x_2},\ldots\mathbf{x_n})$. Note that each function is a function of vectors; i.e. **r** would have 3 components in Cartesian coordinates. When modeling a HEA, the number of electrons can get very large and thus replacing the wave function with $\rho(\mathbf{r})$ speeds up calculations. Closed form solutions do not exist in DFT and only a solutions for small systems are known for the Schrodinger equation. With all this said, the biggest issue is that quantum mechanics is formulated in terms of Ψ, not ρ. However, Hohenberg and Kohn showed that $E = E[\rho(\mathbf{r})]$ exists. This is the energy density functional and while the form isn't known, the relationship does exist. This observation makes DFT possible and allows calculations of energy by simply knowing the electron density of an atom, which is known from orbitals.

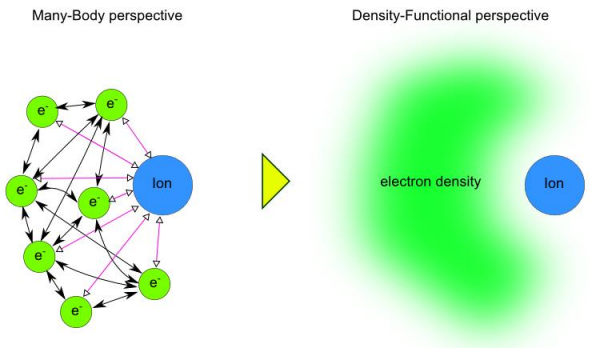

Figure 7: DFT versus Many-Body perspective [103]

The functional is divided into three parts and is analogous to the Hamiltonian.

$$E[\boldsymbol{\rho}(r)] = E_{en}[\boldsymbol{\rho}(r)] + J[\boldsymbol{\rho}(r)] + T[\boldsymbol{\rho}(r)]$$

The first term is the electron nuclear attraction given by

$$E_{en}[\boldsymbol{\rho}(r)] = -\sum_{A}^{nuc} \int \frac{Z_A \rho(r)}{|R_A - r|} dr$$

This is a Coulombic term where the charge of the nuclei (Z) at position (R_A) interacts with the electron density, probed at **r.**

$$J[\boldsymbol{\rho}(r)] = \frac{1}{2} \iint \frac{\rho(r)\rho(r')}{|r - r'|} dr dr'$$

Electron interaction follows the same logic as the nuclear attraction. Two electron densities interact with each other with **r** being the position in the first electron cloud and **r'** being the position of another. The ½ is used to prevent double counting (i.e. interaction AB is equivalent to BA).

$$T = \sum_{i=1}^{N} \langle \Phi_i | -.5\nabla^2 | \Phi_i \rangle$$

The kinetic energy term is found from molecular orbitals which describe the probability of finding an electron at any given position. The orbital is related to the electron density by

$$\rho(r) = \sum_{i=1}^{N} |\Phi_i(r)|^2$$

Two problems exist in these approximations to the total energy. First, employing orbitals to calculate the kinetic energy assumes that the electrons are non-interacting. Secondly, anti-symmetry must be taken into account when describing the repulsion of the electrons. A term called the exchange-correlation energy is added to fix these issues. It is essentially a fudge factor and many forms exist. Today, the Local Density Approximation (LDA) and the Generalized Gradient Approximation (GGA) are the most widely used functionals to correct the energy of the system. Both were found to give comparable results in the calculation of MoNbTaW.

DFT is different from molecular dynamics (MD) in that atomic interactions and total energy of the system is found by approximating solutions to the Schrodinger equation. Reaction dynamics can be observed since electrons are taken into consideration. However, MD neglects quantum effects and calculates energy and reactions by approximating the atoms as classical particles. While this reduces computation time, accuracy is lost by neglecting the wavelike nature found on the atomic scale. Also, accurate classical potentials are difficult to come by when simulating exotic materials.

CHAPTER 4

SIMULATION CONFIGURATION

4.1 Quality

Before beginning simulations, the input parameters were defined. This was accomplished by first selecting values from publications specifically working with transition metals. Convergence criteria for the geometry optimization were less strict than the elastic constant calculations as the weighted average approach for the lattice parameter proved to be quite accurate. As a result, the geometry optimization only changed the lattice parameter of the system by 2-3% regardless of the convergence tolerances. The atomic positions were fixed and only the cell was altered to find equilibrium. The basis set for the variable cell was set to *fixed basis quality* and the compressibility was set to hard. Most of the simulations converged well before the maximum 100 iterations was reached. No external stress was applied. Elastic simulations used an ultrasoft pseudopotential represented in reciprocal space. Specific criteria can be seen in **Table 4-5**.

Table 4: Convergence criteria for geometry optimization

Convergence Parameter	Value
Energy	2.0e-5 eV/atom
Max Force	.05 eV/A
Max Stress	.1 GPa
Max Displacement	.002 A
Max Iterations	100

Table 5: Convergence criteria for elastic constant calculation

Convergence Parameter	Value
Energy Cutoff	320 eV
SCF Tolerance	1e-6 eV/A
Max SCF Cycles	100
k-point Grid	.4x8x8
Energy Tolearnce	Per atom, not cell

Table 6: Computer specifications for system used in research

Computer Specifications	
Processor	Intel Xeon CPU E5-2670 v2 @ 2.5 GHz
Installed Memory	128 GB
System Type	64-bit OS

4.2 Validation via Known Systems

4.21 Pure Metal

Before simulating high entropy systems that have not yet been fabricated, the functionals and convergence criteria must be applied to known systems of varying sizes in order to have any validity. Pure metals have been studied extensively and have properties that are well defined. Molybdenum is known to have an Im3m crystal type and a lattice parameter of 3.147 angstroms. These accepted parameters were used to create a molybdenum cell in a 3D atomistic document

(**Figure 8**). The lattice parameters post geometry optimization grew to 3.16 A, only .4% error. Simulated elastic values were 316 GPa for the elastic modulus and 228 GPa for the bulk modulus which were close to the accepted values of 329 GPa and 230 GPa, respectively. Computational time was less than a minute for both the geometry optimization and elastic constant calculations since only two atoms were used. Creation of a supercell is not necessary and does not change the data much as the number of atoms is increased.

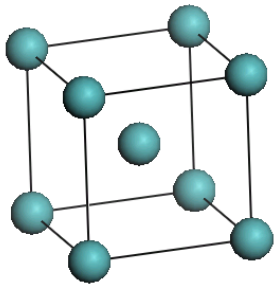

Figure 8: Molybdenum unit cell

4.23 Quaternary

FeCrCoNi is a FCC HEA that was studied by Tian (2013). This cell was reproduced and run in CASTEP to compare elastic properties. 13% error was seen in C44, a diagonal elastic constant. The error most likely stemmed from using too few atoms which did not truly represent the isotropic behavior of the system. Convergence tests were performed on MoNbTaW to ensure that the elastic properties in all three coordinate directions were similar in value. **Table 7** shows the reported and calculated values for the unit cell that can be seen in **Figure 9**.

Table 7: Reported vs. simulated elastic values in FeCrCoNi

Property	Reported Value	Calculated Value
Bulk Modulus	207 GPa	190 GPa
C44	189 GPa	163 GPa
C12	175 GPa	168 GPa

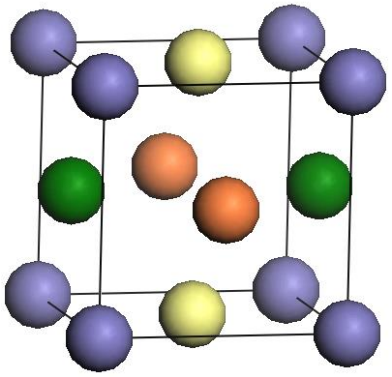

Figure 9: FeCrCoNi unit cell

CHAPTER 5

SYSTEM CONFIGURATION

5.1 Design Parameters

5.11 Phase Diagrams

Phase diagrams provide information about what microstructures are to be expected when different elements are brought together under varying temperatures and pressures. **Appendix A** shows phase diagrams for the possible 10 binary combinations of elements in MoNbTaTiW. It can be seen that a BCC_A2 phase (Im3m) is represented in each diagram over most temperature and concentration ranges. If each of the elements were to be alloyed, it is highly unlikely that a phase would exist that is not present on the diagrams. Intermetallic phases could still develop, but the following two design parameters minimize that chance.

5.12 Hume-Rothery

The Hume-Rothery rules state the atomic size differences among elements should be less than 15% in order to form a solid solution. From **Table 8**, it can be seen that there is a 16.9% difference between the atomic sizes of Ta and V. All other binary pairs fall within the specified limit. It can also be seen that there are no large differences in electronegativities. While there is no strict adherence to the Hume-Rothery rules, HEAs do not necessarily have to meet all the criteria in order to form a solid solution. A more precise guideline is given in the following section.

Table 8: Atomic size and electronegativity data for the elements

Element	Atomic Size (pm)	Electronegativity
Mo	190	2.16
Nb	198	1.60
Ta	200	1.50
W	193	2.36
Ti	176	1.54
V	171	1.63

5.13 Mixing Enthalpy Considerations

Troparevsky et al. [93] proposed a simple predictive method, which solely relies on enthalpy of formation data to determine which elements will combine to form single-phase alloys. Specifically, if every binary's enthalpy of formation falls within a set range, a single phase is expected. Enthalpy of formation data can be found in alloy databases or calculated using computational methods such as DFT. Most elemental pairs have negative enthalpies of formation indicating an exothermic process. Complex compounds are unlikely to form in HEAs due to slow diffusion of the alloying elements under proper annealing, therefore, it is reasonable to consider only the binaries. The method proposed by Troparevsky et al. accurately predicts single phase HEAs that have been experimentally proven and rejects systems that form intermetallics or multiple phases. The range that binaries must fall into in order to form a single phase is set by $-T_{ann}\Delta S_{mix}$ and the largest value of ΔH_f for which the alloy does not phase separate. This range ensures that the system is neither too stable in which compounds could precipitate, nor unstable in which the constituent elements would not mix at all. Specifically, the upper range is 37meV and

is chosen as it includes all known single-phase alloys. Both the lower and upper limits are justified as follows: solid solution alloys with multiple components typically show small enthalpies of formation and ordered compounds generally present small entropic terms. As stated above, only data from binary combinations need to be calculated and fall within the given range.

For modeling considerations, the annealing temperature to set the minimum value of the range can be approximated by substituting a critical temperature for the annealing temperature. This critical temperature can be approximated as $.6T_m$ where T_m is the average melting temperature of the constituent elements. Taking this specific fraction of the average melting temperature is consistent with experimental annealing temperatures [93].

Table 9: Melting temperatures for base elements

Element	Melting Temperature (C)
Molybdenum	2623
Niobium	2477
Tantalum	3017
Titanium	1668
Tungsten	3422
Average	**2641**

Assume $.55T_m$ is equivalent to T_{ann} for a tighter range of mixing enthalpies. T_{ann} is then equal to 1452K for the MoNbtaTiW system when using the average melting temperatures for T_m. To find the value for mixing enthalpy, the equation below can be used.

$$\Delta S_{mix} = -nR \Sigma_i (x_i \ln x_i)$$

ΔS_{mix} for a system of 5 constituent elements in equal atomic proportion is equal to .1387 after converting to units of meV/Katom. Finally, solving $-T_{ann}\Delta S_{mix}$ yields a lower limit of -201.4 meV/atom. Therefore, every binary combination should have a mixing enthalpy that falls within

the range of -201.4 meV < ΔH_f < 37 meV. Indeed, all of the binaries fall within this range as can be seen in the table below. Note that all of the binaries are within the range when substituting titanium with vanadium.

Table 10: Enthalpies of formation for binary systems

Binary	Enthalpy of Formation (meV)
MoNb	-133
MoTa	-193
MoTi	-167
MoW	-8
NbTa	-10
NbTi	11
NbW	-76
TaTi	31
TaW	-114
TiW	-82

5.2 Determination of System Size

The number of atoms used in each simulation needs to be enough so that the cell is representative of a random solid solution, yet not too large that the system takes days or weeks to finish. In order to find the optimum size, various sized supercells of MoNbTaW were simulated and the elastic moduli plotted to find the convergence point. The alloy is expected to be isotropic and thus, the Young's modulus in each of the Cartesian coordinate directions should be very similar in value. From the plot, the x, y, and z values all converge to approximately 295 GPa as the number of atoms in the system exceed 16.

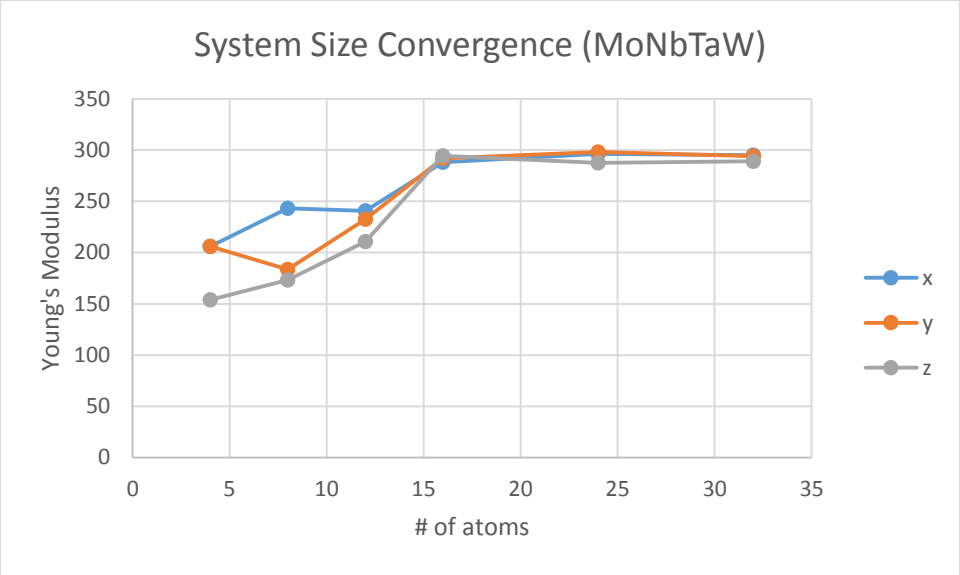

Figure 10: Convergence of elastic moduli for each Cartesian coordinate

To ensure convergence of the elastic moduli, all subsequent simulations were performed on supercells with at least 16 atoms. The exact number of atoms used had to be adjusted depending on the concentration of titanium or vanadium that was being investigated. It was not possible to represent titanium at 11.1%, 20%, 25%, etc. in the same sized cell. **Table 11** shows the number of atoms that were used for each percentage. For example, to represent titanium at 25% required a ratio of 4:3:3:3:3 in MoNbTaWTi25. **Figure 11** shows the approximate simulation times for different sized systems.

Table 11: System size required for each composition

Percent of Ti/V	# of atoms
0	32
11.1	36
20	20
25	16
33.3	24

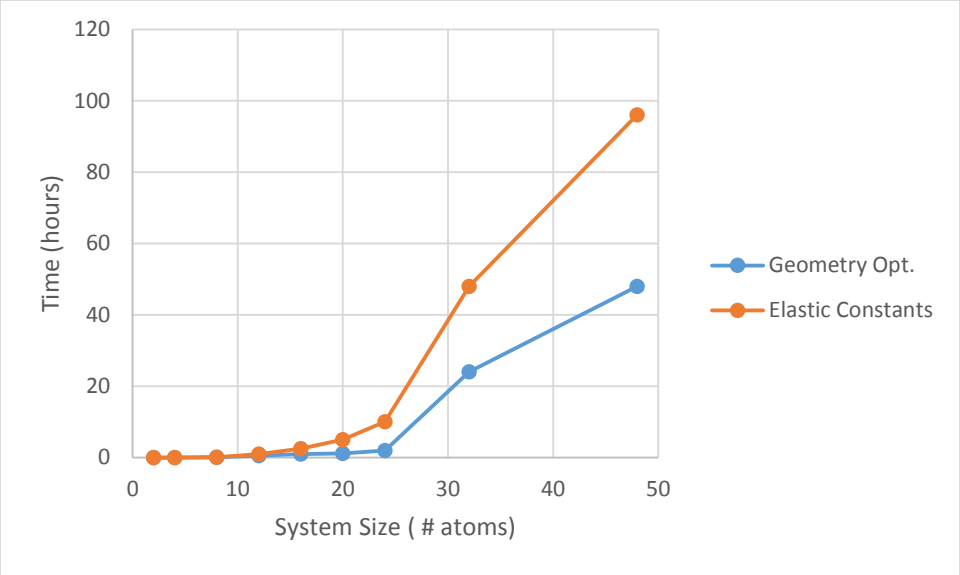

Figure 11: Approximate simulation time

5.3 Proof of Linear Elasticity

Metals and alloys, including high entropy alloys, are expected to exhibit linear elasticity. If theoretical calculations show behavior that is not consistent with this notion, then Hooke's Law is not applicable and the data is not valid. The quasi-static strain amplitude was adjusted multiple times and the modulus of elasticity did not change for MoNbTaW, MoNbTaWTi or MoNbTaWV. Specifically, the maximum strain amplitude was varied between .003, .03 and .3 without any effect on the elastic properties. All of the simulations were performed with a quasi-static strain amplitude of .03 to ensure that the material was in the linear elastic range.

5.4 Comparison of Random Configurations

If MoNbTaW were to be arc melted and allowed to cool, the atoms are predicted to form a solid solution in a BCC lattice. Where each individual atom goes will be probabilistic in nature due to quantum effects at the subatomic level. If the same material were to be melted and cooled a second time, the atoms would be in a different arrangement. Many properties are invariant even

though the solution is random because the atomic bonding is the sole variable. In order to prove this, an Im3m supercell was set up with 32 atoms. The Young's modulus varied only slightly when the atoms were placed in different positions.

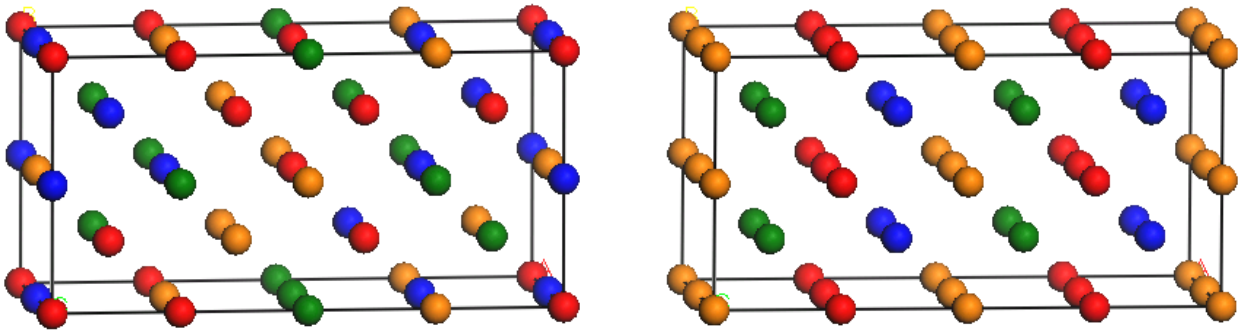

Young's Modulus = 294 GPa

Young's Modulus = 290 GPa

Figure 12: Two configurations of a MoNbTaW supercell

CHAPTER 6

EFFECT OF INCREASING TITANIUM AND VANADIUM CONCENTRATION

Simulations calculated a Young's modulus of 292 GPa for MoNbTaW. The corresponding elemental values are 330, 105, 186 and 400 GPa, respectively, yielding an average of 255 GPa. This suggests that the HEA experiences solid solution strengthening. Adding titanium to this quaternary system showed a linear decrease with a coefficient of determination of .98. Titanium's elastic modulus is 110 GPa, therefore an increase in ductility is justified. Increasing the concentration of vanadium also yielded a downward trend, however it was not linear. There was little difference in MoNbTaW and $MoNbTaWV_{11\%}$ and no difference between $MoNbTaWV_{25\%}$ and $MoNbTaWV_{33\%}$. However, a decrease was seen in concentrations ranging from 11% to 25%. This is most likely due to the cocktail effect having more influence than solid solution strengthening in that range. **Figures 13-14** show plots of C11 and C22 as titanium and vanadium are added to the base system. The elastic constants form a 6x6 matrix and are calculated from Hooke's Law. The strain amplitude is given by the user and forms the 3x3 strain tensor which CASTEP uses to perturb the system. Stress is then easily calculated from the change of energy. Therefore, the elastic stiffness tensor is the only unknown.

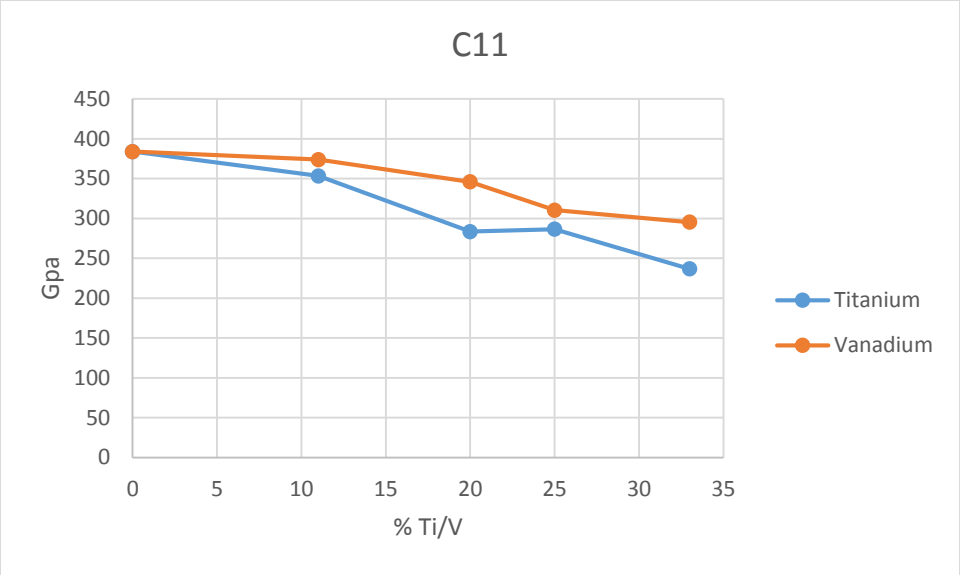

Figure 13: Effect of Ti and V on C11 in MoNbTaW

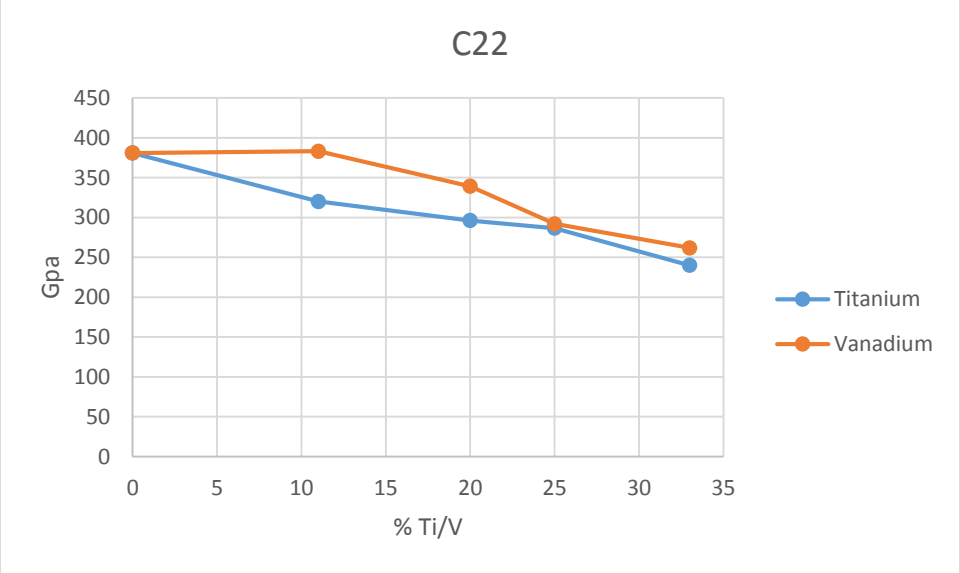

Figure 14: Effect of Ti and V on C22 in MoNbTaW

Figures 15 and **16** shows how the Young's Modulus changes when adding Ti and V, respectively. Addition of Ti yielded a linear decrease in the elastic modulus over the range of 0% to 33%. The coefficient of determination was roughly .98. This is a strong correlation and it would be a good assumption that any concentration of Ti below 33% could be predicted based on this graph. The curve will either smooth out at some point beyond 33% to Ti's elastic modulus or break down completely when phase separation occurs. Addition of V didn't change when represented at 11% or in the range of 25-33%. More simulations need to be performed at varying concentrations to draw any real conclusions. However, a downward trend was seen.

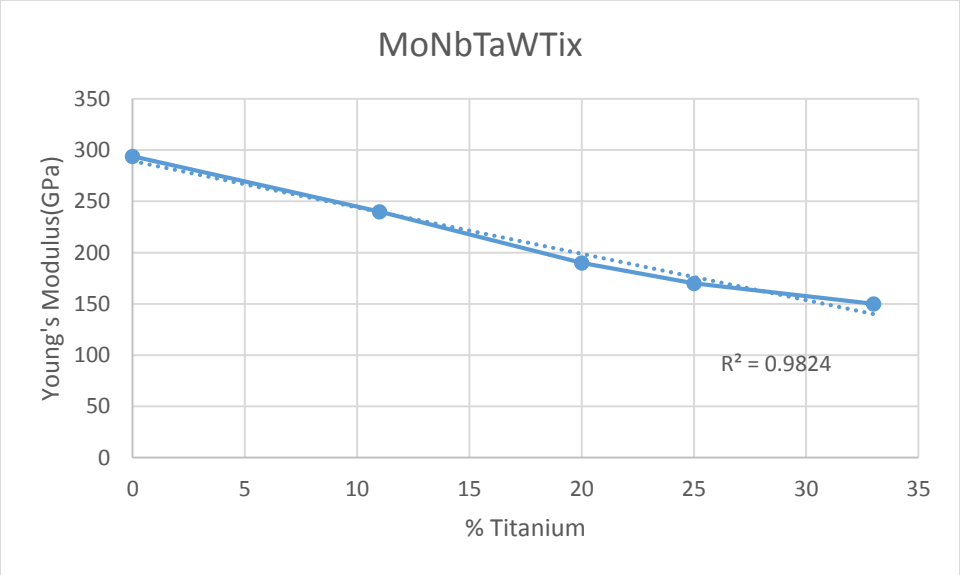

Figure 15: Young's Modulus vs. % Ti alloyed in MoNbTaW

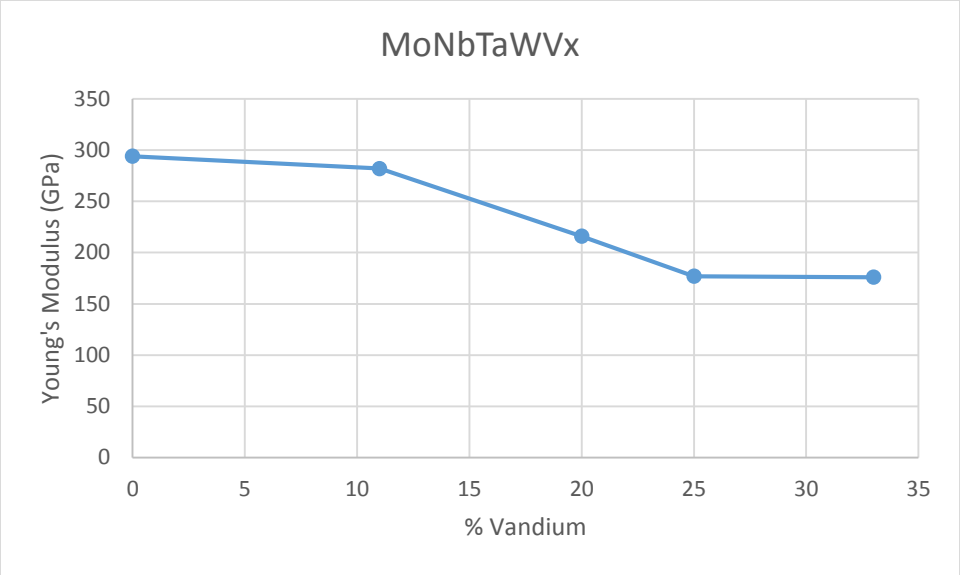

Figure 16: Young's Modulus vs. % V alloyed in MoNbTaW

The values for Young's Modulus, as well as the bulk and shear modulus, was found by taking the inverse of the stiffness tensor to yield the elastic compliance tensor. Then simple equations were employed to find the needed values (see below).

$$\text{Modulus of Elasticity} = \frac{1}{S_{11}} = \frac{1}{.0033881} = 295.15 \text{ GPa}$$

$$\text{Bulk Modulus} = \frac{1}{(S_{11}+S_{22}+S_{33})+2(S_{12}+S_{13}+S_{23})} = 229.45 \text{ GPa}$$

$$\text{Shear Modulus} = \frac{1}{4(S_{11}+S_{22}+S_{33})-4(S_{12}+S_{13}+S_{23})+3(S_{44}+S_{55}+S_{66})} = 94.24 \text{ GPa}$$

Figures 17-18 show the bulk and shear modulus, respectively. A downward trend is again seen as all of the elastic properties are related.

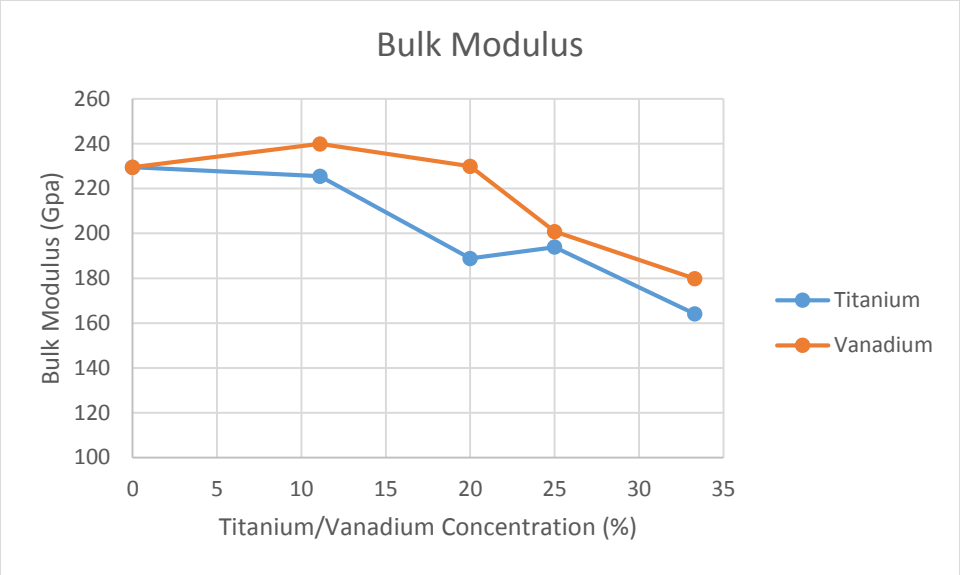

Figure 17: Bulk Modulus vs. % of Ti/V in MoNbTaW

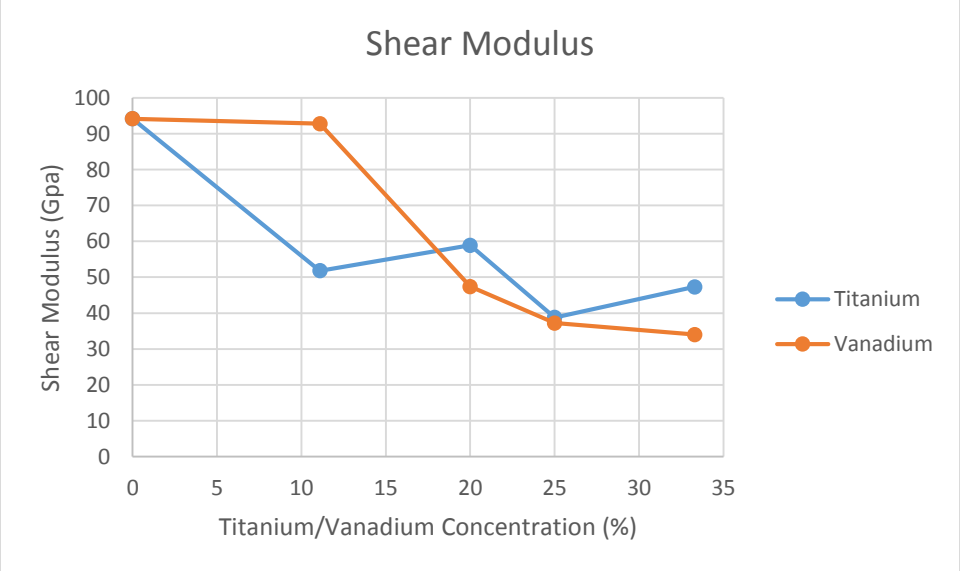

Figure 18: Shear Modulus vs. % of Ti/V in MoNbTaW

High elastic moduli correspond to strong bonds, therefore it is possible to predict melting temperatures from the simulated values. **Figure 19** shows an Ashby plot of Young's Modulus versus melting point. With the exception of lead, the metals and alloys follow a somewhat linear increase in melting point as the elastic modulus is increased. Many of the systems studied in this research are predicted to have melting temperatures that rival nickel based super alloys (see **Table 12**).

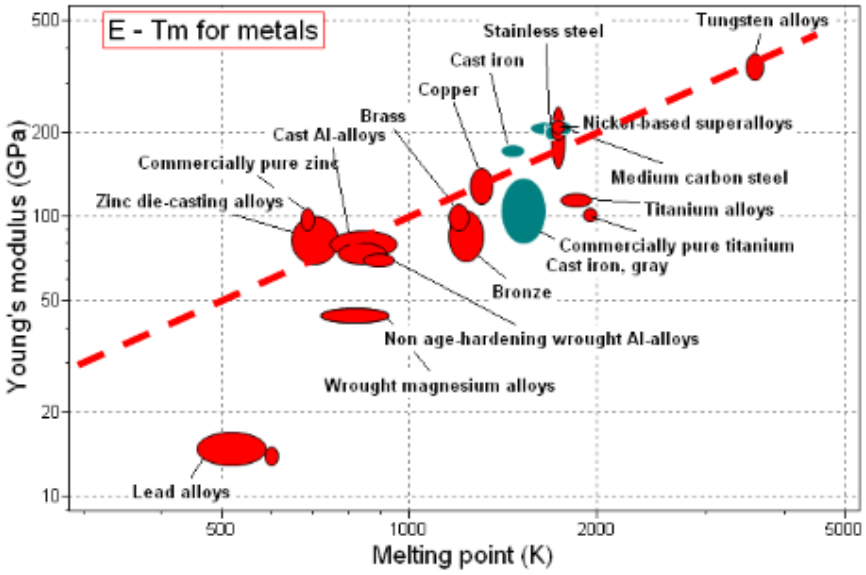

Figure 19: Young's Modulus and melting point for various metals/alloys

Table 12: Expected melting temperatures from Young's Modulus

MoNbTaW	≈ 3000K
$MoNbTaWTi_{11\%}$	≈ 2500K
$MoNbTaWTi_{20\%}$	≈ 1900K
$MoNbTaWV_{11\%}$	≈ 2900K
$MoNbTaWV_{20\%}$	≈ 2100K
Nickel Super Alloy	≈ 1900K

CHAPTER 7

CONCLUSIONS

HEAs are an exciting new research area in materials science and many alloys have been fabricated which have favorable properties. There are estimated to be 10^{102} different alloy systems that could potentially be useful to society. This research provides a pathway to limit this number and guide experimental procedure. Software employing Density Functional Theory can quickly determine if a system is likely to be stable as well as calculate many material properties. Further time and money can be saved when inverse material design becomes more common. If a specific combination of properties is needed for an application, the inverse approach means going to the periodic table and choosing which elements will provide the needed specifications. Pairing both this inverse philosophy and DFT will save much time in the laboratory.

Nickel super alloys are the popular choice in today's high temperature applications where ductility is also a concern. While these alloys perform very well, a material with even higher operating temperatures while maintaining ductility would increase the efficiency in turbine engines and waste incinerators. The high entropy alloy that was studied consisted of Mo, Nb, Ta, Ti and W in equal atomic proportion. The refractory metals provide high temperature strength and Ti confers properties such as corrosion resistance and low density. Each of these elements have similar atomic size and BCC lattices (Ti is HCP at room temperature). Analysis of each possible binary phase diagram shows that an Im3m space group will be present. It will be assumed that the HEA will form a single-phase solution with a BCC lattice. It is possible, yet very unlikely, that an

intermetallic phase could be present when actually fabricating the alloy. An alternative route to determine the structure of an unknown material is to setup a collection of tens of thousands of atoms and perform simulated annealing. To do this, a program is written to randomly place atoms using Cartesian coordinates and then heat up (increase the kinetic energy) the material well beyond the melting temperature of W (highest melting temperature of the constituents). This ensures that nearest neighbor interactions are eliminated. The energy is calculated using DFT or some other type of first principal approach. This approach is time consuming and is not necessary when thermodynamic data is available. Currently, mixing enthalpy considerations put forth by Troparevsky et al. [93] provide the most reliable predictive method of determining solubility. Simulations calculated a Young's Modulus of 292 GPa for MoNbTaW and many of the systems studied are predicted to have melting temperatures that rival that of nickel super alloys.

Computer simulations will only be as accurate as the information that is provided by the user. Before running any type of quantum mechanical or molecular dynamic software, the system must be generated. In the case of CASTEP, the user is required to provide the space group and lattice parameters when creating a crystal. The space group used was Im3m, consistent with the binary phase diagrams. Lattice parameters were adjusted when a geometry optimization was ran, so this parameter is not as a critical as the space group. However, a carefully chosen lattice parameter can help the simulation converge more quickly. A weighted average approach yields 3.142 A and is usually very close to the actual lattice parameter of a crystal.

LIST OF REFERENCES

[1] Vincent, A.J.B. A study of three multicomponent alloys. BSc Part II Thesis, University of Sussex, UK, 1981

[2] Cantor, B.; Chang, I.T.H.; Knight, P.; Vincent, A.J.B. Microstructure development in equiatomic multicomponent alloys. *Mater. Sci. Eng. A, 2004, 375, 213–218*

[3] Zhang, Y.; Zuo, T.; Tang, Z. Microstructures and properties of high entropy alloys. *Progress in Materials Science, 2004*

[4] Khaled M. Youssef, Qatar University; Alexander J. Zaddach, Changning Niu, Douglas L. Irving, and Carl C. Koch. A Novel Low Density, High Hardness, High-Entropy Alloy with Close-packed Single-phase Nanocrystalline Structures. North Carolina State University. Dec. 9, *Materials Research Letters*

[5] Shizhong Yang, Mohammad Hamed Habibi, Li Wang, Shengmin Guo, Zhi Tang, Peter Liaw, Liuxi Tan, Cheng Guo, Michael Jackson. The Hot Corrosion Resistance Properties of AlxFeCoCrNi. *2014 TMS Annual Meeting and Exhibition*

[6] Yeh JW, Chen SK, Lin SJ, Gan JY, Chin TS, Shun TT. Nanostructured high-entropy alloys with multiple principal elements: novel alloy design concepts and outcomes. *Adv Eng Mater, 2004*

[7] Zhang Y, Yang X, Liaw PK. Alloy design and properties optimization of high-entropy alloys. *JOM, 2012, Volume 64, Issue 7*

[8] Yeh JW. (2006) Recent progress in high-entropy alloys. *Ann Chim Sci Mater.*

[9] Donaldson, S. (2011). Entropy is not disorder. *Retrieved from http://www.science20.com/train_thought/blog/entropy_not_disorder-75081*

[10] Cantor, Brian. Multicomponent and High Entropy Alloys. *Entropy 2014, 16, 4749-4768*

[11] Illustrated Glossary of Organic Chemistry (Accessed July 2015). Retrieved from *http://www.chem.ucla.edu/~harding/IGOC/E/electron_density.html*

[12] Cuevas, J. (Accessed June 2015) Introduction to Density Functional Theory. Retrieved from *https://www.uam.es/personal_pdi/ciencias/jcuevas/Talks/JC-Cuevas-DFT.pdf*

[13] Gao, Michael C.; Alman, David E. Searching for the Next Single-Phase High-Entropy Alloy Compositions. *Entropy, 10/2013, Volume 15, Issue 10*

[14] Senkov, O.N.; Wilks, G.B.; Miracle, D.B.; Chuang, C.P.; Liaw, P.K. Refractory high-entropy alloys. *Intermetallics 2010, 18, 1758–1765*

[15] Senkov, O.N.; Wilks, G.B.; Scott, J.M.; Miracle, D.B. Mechanical properties of Nb25Mo25Ta25W25 and V20Nb20Mo20Ta20W20 refractory high entropy alloys. *Intermetallics 2011, 19, 698–706.*

[16] Senkov, O.N.; Scott, J.M.; Senkova, S.V.; Miracle, D.B.; Woodward, C.F. Microstructure and room temperature properties of a high-entropy TaNbHfZrTi alloy. *J. Alloys Comp. 2011, 509, 6043–6048.*

[17] Chen, Y.-L.; Tsai, C.-W.; Juan, C.-C.; Chuang, M.-H.; Yeh, J.-W.; Chin, T.-S.; Chen, S.-K. Amorphization of equimolar alloys with HCP elements during mechanical alloying. *J. Alloys Comp. 2010, 506, 210–215.*

[18] Tsai, Ming-Hung. Physical Properties of High Entropy Alloys. *Entropy, 12/2013, Volume 15, Issue 12*

[19] M D Segall1, Philip J D Lindan, M J Probert, C J Pickard,PJ Hasnip, S J Clark and M C Payne. First-principles simulation: ideas, illustrations and the CASTEP code. 2002

[20] Introduction to space groups (Accessed September 2015). Retrieved from *http://pd.chem.ucl.ac.uk/pdnn/symm3/sgintro.htm*

[21] Tsau. Chang. Microstructures and Mechanical Properties of TiCrZrNbNx Alloy Nitride Thin Films. 2013

[22] Lin, Shao-Yi; Chang, Shou-Yi; Chang, Chia-Jung; Huang, Yi-Chung. Nanomechanical Properties and Deformation Behaviors of Multi-Component (AlCrTaTiZr)NxSiy High-Entropy Coatings. *Entropy, 01/2014, Volume 16, Issue 1*

[23] Chen, Shu Ying; Yang, Xiao; Dahmen, Karin A; Liaw, Peter K; Zhang, Yong Microstructures and Crackling Noise of AlxNbTiMoV High Entropy Alloys. *Entropy, 02/2014, Volume 16, Issue 2*

[24] Yeh, W. Tsai, Y. Tsai, H. Sluggish diffusion in CoCrFeMnNi high-entropy alloys. *Acta Materialia 61(13):4887–4897, July 2013*

[25] Ravelo R, Aguilar J, Baskes M, Angelo JE, Fultz B, Holian BL. Free energy and vibrational entropy difference between ordered and disorderd Ni3Al. *Physical Review B - Condensed Matter and Materials Physics, 01/1998, Volume 57, Issue 2*

[26] Wang FJ, Zhang Y, Chen GI, Davies HA. Tensile and compressive mechanical behavior of a CoCrCuFeNiAl high entropy alloy. *International Journal of Modern Physics B, Volume 23, Issue 06-07, pp. 1254-1259 (2009)*

[27] Wang XF, Zhang Y, Qio Y, Chen GL. Novel microstructure and properties of multicomponent CoCrCuFeNiTi alloys. *Intermetallics, 2007, Volume 15, Issue 3*

[28] Zhou YJ, Zhang Y, Wang YI, Chen GI. Solid solution alloys of AlCoCrFeNiTi, with excellent room-temperature mechanical properties. *Applied Physics Letters, 2007, Volume 90, Issue 18*

[29] Zhang Y, Zuo T, Cheng Y, Liaw PK. High entropy alloys with high saturation magnetization, electrical resistivity and malleability. *Scientific Reports, 2013, Volume 3*

[30] Hemphill, MA. Yuan, T. Wang, GY. Yeh, JW. Tsai, CW. Chuang, A. Liaw, PK. Fatigue behavior of Al.5CoCrCuFeNi high entropy alloys. *Acta Materialia, 09/2012, Volume 60, Issue 16*

[31] Chen, YI. Tsai, CW. Juan, CC. Chuang, MH. Yeh, JW. Chin, TS. Amorphization of equimolar alloys with HCP elements during mechanical alloying. *Journal of Alloys and Compounds, 2010, Volume 506, Issue 1*

[32] Yao, CZ. Zhang, P. Liu, M. Li, GR. Ye, JQ. Liu, P. Electrochemical preparation and magnetic study of BiFeCoNiMn high entropy alloy. *Electrochimica Acta, 2008, Volume 53, Issue 28*

[33] What is Induction Heating? (Accessed December 2015). Retrieved from *http://www.gh-ia.com/induction_heating.html*

[34] Wang, FJ. Zhang, Y. Chen, GI. Davies, HA. Cooling rate and size effect on the microstructure and mechanical properties of AlCoCrFeNi high entropy alloy. *Journal of Engineering Materials and Technology, 07/2009, Volume 131, Issue 3*

[35] Senkov, O.N.; Zhang, F.; Miller, J.D. Phase composition of a $CrMo_{0.5}NbTa_{0.5}TiZr$ high entropy alloy: Comparison of experimental and simulated data. *Entropy 2013, 15, 3796–3809.*

[36] Chuang, M.H.; Tsai, M.H.; Wang, W.R.; Lin, S.J.; Yeh, J.W. Microstructure and wear behavior of $Al_xCo_{1.5}CrFeNi_{1.5}Ti_Y$ high-entropy alloys. *Acta Mater. 2011, 59, 6308–6317.*

[37] Huhn, William P.; Widom, Michael. Prediction of A2 to B2 Phase Transition in the High-Entropy Alloy Mo-Nb-Ta-W. *JOM, 12/2013, Volume 65, Issue 12*

[38] Lucas, M.S; Wilks, G.B; Mauger, L; Muñoz, J.A; Senkov, O.N; Michel, E; Horwath, J; Semiatin, S.L; Stone, M.B; Abernathy, D.L; Karapetrova, E. Absence of long-range chemical ordering in equimolar FeCoCrNi. *Applied Physics Letters, 06/2012, Volume 100, Issue 25*

[39] Ranganthan, S. Multimaterial cocktails. *Curr. Sci. 2003, 85, 1404*

[40] Wang, X.-R; He, P; Lin, T.-S; Wang, Z.-Q. Microstructure, thermodynamics and compressive properties of AlCoCrCuMn-X (x=Fe, Ti) high-entropy alloys. Materials and Science Engineering. *Materials Science and Technology (United Kingdom), 12/2015, Volume 31, Issue 15*

[41] Zhang, Y.; Zuo, T.; Cheng, Y.; Liaw, P.K. *Sci Rep., 3 (2013) pg. 1455*

[42] Yang, X.; Zhang, Y. Prediction of high-entropy stabilized solid-solution in multi-component alloys. *Materials Chemistry and Physics, 02/2012, Volume 132, Issue 2-3*

[43] Juan, Chien-Chang; Tsai, Ming-Hung; Tsai, Che-Wei; Lin, Chun-Ming; Wang, Woei-Ren; Yang, Chih-Chao; Chen, Swe-Kai; Lin, Su-Jien; Yeh, Jien-Wei. Enhanced mechanical properties of HfMoTatiZr and hfMoNbTaTiZr refractory high-entropy alloys. *Intermetallics Vol 62. 2015*

[44] H. Hirai, T. Tabaru, H. Ueno, A. Kitahara, S. Hanada. Microstructures and mechanical properties of directionally solidified Nb-xMo-22Ti-18Si in-situ composites. *J Jpn Inst Met, 64 (2000), pp. 474–480*

[45] J.W. Yeh. Alloy design strategies and Future trends in high-entropy Alloys. *JOM, 65 (2013), pp. 1759–1771*

[46] Ji, Wei; Wang, Yucheng; Wang, Weimin; Wang, Hao; Zhang, Jinyong; Zhang, Fan; Fu, Zhengyi. Alloying behavior and novel properties of CoCrFeNiMn high-entropy alloy fabricated by mechanical alloying and spark plasma sintering. *Intermetallics Vol 56. 2015*

[47] Stepanov, N.D; Shaysultanov, D.G; Salishchev, G.A; Tikhonovsky, M.A; Oleynik, E.E; Tortika, A.S; Senkov, O.N. Effect of V on microstructure and mechanical properties of the CoCrFeMnNiVx HEAs. *Journal of Alloys and Compounds, 04/2015, Volume 628*

[48] Stepanov, N; Tikhonovsky, M; Yurchenko, N; Zyabkin, D; Klimova, M; Zherebtsov, S; Efimov, A; Salishchev, G. Effect of cryo-deformation on structure and properties of CoCrFeNiMnHEA. *Intermetallics Vol 59. 2015*

[49] J.-W. Yeh, S.-J. Lin, T.-S. Chin, J.-Y. Gan, S.-K. Chen, T.-T. Shun, et al. Formation of simple crystal structures in Cu–Co–Ni–Cr–Al–Fe–Ti–V alloys with multiprincipal metallic elements. *Metall Mater Trans A, 35 (2004), pp. 2533–2536*

[50] C.-J. Tong, M.-R. Chen, J.-W. Yeh, S.-J. Lin, S.-K. Chen, T.-T. Shun, et al. Mechanical performance of the AlxCoCrCuFeNi high-entropy alloy system with multiprincipal elements. *Metall Mater Trans A, 36 (2005), pp. 1263–1271*

[51] C.-J. Tong, Y.-L. Chen, J.-W. Yeh, S.-J. Lin, S.-K. Chen, T.-T. Shun, et al. Microstructure characterization of AlxCoCrCuFeNi high-entropy alloy system with multiprincipal elements. *Metall Mater Trans A, 36 (2005), pp. 881–893*

[52] M.-R. Chen, S.-J. Lin, J.-W. Yeh, S.-K. Chen, Y.-S. Huang, C.-P. Tu. Microstructure and properties of Al0.5CoCrCuFeNiTix(x=0–2.0) high-entropy alloys. *Mater Trans, 47 (2006), pp. 1395–1401*

[53] S. Singh, N. Wanderka, B.S. Murty, U. Glatzel, J. Banhart. Decomposition in multi-component AlCoCrCuFeNi high-entropy alloy. *Acta Mater, 59 (2011), pp. 182–190*

[54] Nayan, Niraj; Singh, Gaurav; Murty, S.V.S.N; Jha, Abhay K; Pant, Bhanu; George, Koshy M; Ramamurty, Upadrasta. Hot deformation behavior and microstructure control in AlCrCuNiFeCo high entropy alloy. *Intermetallics Vol 55. 2014*

[55] A.V. Kuznetsov, D.G. Shaysultanov, N.D. Stepanov, G.A. Salishchev, O.N. Senkov. Tensile properties of an AlCrCuNiFeCo high-entropy alloy in as-cast and wrought conditions. *Mater Sci Eng A, 533 (2012), pp. 107–118*

[56] Y.V.R.K. Prasad, S. Sasidhara. Hot working guide: a compendium of processing maps. *ASM International, Materials Park, OH (1997)*

[57] Kunce, I. Microstructural characterisation of high-entropy alloy AlCoCrFeNi fabricated by laser engineered net shaping. *Intermetallics Vol 648. 2015*

[58] H. Chen, A. Kauffmann, B. Gorr, D. Schliephake, C. Seemuller, J. Wagner, H. Christ, M. Heilmaier. Microstructure and mechanical properties at elevated temperatures of a new Al-containing refractory high-entropy alloy Nb-Mo-Cr-Ti-Al. *Journal of Alloys and Compounds. March 2016 Vol 661.*

[59] O. Senkov, S. Senkova, C. Woodward, D.B. Miracle. Low-Density, refractory multi-principal element alloys of the Cr-Nb-Ti-V-Zr system: microstructure and phase analysis. *Acta Mater. 2013 pp. 1545-1557*

[60] B. Gorr, M. Azim, H.J. Christ, T. Mueller, D. Schliephake, M. Heilmaier. Phase equilibria, microstructure and high temperature oxidation resistance of novel refractory high-entropy alloys. *J. Alloys Compd. 624 (2014). Pp. 270-278*

[61] O.N. Senkov. S.L. Semiatin. Microstructure and properties of a refractory high-entropy alloy after cold working. *J Alloys Compd. 649 (2015)*

[62] B. Schuh, F. Mendez-Martin, B. Volker, E.P. George, et al. Mechanical properties, microstructure and thermal stability of a nanocrystalline CoCrFeMnNi high-entropy alloy after severe plastic deformation. *Acta Materialia. Vol 96. Pp. 258-268*

[63] F. Otto, A. Dlouhy, Ch. Somsen, H. Bei, G. Eggeler, E.P George. The influences of temperature and microstructure on the tensile properties of a CoCrFeMnNi high-entropy alloy. *Acta Mater., 61 (2013) pp. 5743-5755*

[64] A. Gali, E.P. George. Tensile properties of high and medium entropy alloys. *Intermetallics, 39 (2013), pp. 74-78*

[65] F. Meng, I. Baker. *Journal of Alloys and Compounds. Vol 645 pp. 376-381*

[66] Laurent-Brocq, M. Akhatove, A. et al. Insights into the phase diagram of the CrMnFeCoNi high entropy alloy. *Acta Materialia (Vol. 88) 2015*

[67] Strange, John. The Palestinian City-States of the Bronze Age. A comparative study of thirty city-state cultures: an investigative volume. *Vol 21. 2000*

[68] "A Brief History of Iron and Steel" (Accessed 10/9/15). Retrieved from *http://www.anselm.edu/homepage/dbanach/h-carnegie-steel.htm.*

[69] The Discovery of Stainless Steel. (Accessed October 2015). Retrieved from *http://www.bssa.org.uk/about_stainless_steel.php?id=31*

[70] O. Grassel, L. Kruger, G. Frommeyer, L.W. Meyer. High strength Fe-Mn-(Al, Si) TRIP/TWIP steels development – properties – applications. *Int. J. Plast, 16 (2000), pp.1391-1409*

[71] F. Sun, J.Y. Zhang. A new titanium alloy with a concentration of high strength, high strain hardening and improved ductility. *Scr. Mater., 94 (2015), pp.17-20*

[72] Kozak, Roksolana; Sologubenko, Alla; Steurer, Walter. Single phase high entropy alloys. *Zeitschrift fur Kristallographie, 01/2015, Volume 230, Issue 1*

[73] Z. Wang, Q. Weifeng, Y. Yang, C.T. Liu. Atomic-size and lattice-distortion effects in newly developed high-entropy alloys with multiple principal elements. *Intermetallics Vol 64. 2015*

[74] F. Tian, L. Delczeg, N. Chen, L.K. Varga, J. Shen, L. Vitos. Structural stability of NiCoFeCrAlx high-entropy alloy from ab initio theory. *Phys Rev B, 88 (2013), p. 085128*

[75] F, Tian, L.K. Varga, N. Chen, L. Delczeg, L. Vitos. Ab initio investigation of high-entropy alloys of 3 d elements. *Phys Rev B, 87 (2013), p. 075144*

[76] N.I. Kourov, V.G. Pushin, A.V. Korolev, V. Knyazev, M. Ivchenko, M. Ustyugov. Peculiar features of physical properties of the rapid quenched AlCrFeCoNiCu high-entropy alloy. *Journal of Alloys and Compounds. Vol 636 (2015)*

[77] K.B. Zhang, Z.Y. Fu, J.Y. Zhang, J. Shi. Annealing on the structure and properties evolution of the CoCrFeNiCuAl high-entropy alloy. *Journal of Alloys and Compounds. Vol 502 (2010)*

[78] S. Singh, N. Wanderka, K. Kiefer, K. Siemensmeyer, J. Banhart. Effect of decomposition of the Cr–Fe–Co rich phase of AlCoCrCuFeNi high entropy alloy on magnetic properties. *Ultramicroscopy. Vol 111 (2011)*

[79] X. Li, F. Tian, S. Schonecker, J. Zhao, L. Vitos. Ab initio-predicted micro-mechanical performance of refractory high-entropy alloys. *Scientific Reports (July 2005)*

[80] Senkov, O. N. & Woodward, C. F. Microstructure and properties of a refractory NbCrMo0.5Ta0.5TiZr alloy. *Mater. Sci. Eng. A529,311–320 (2011)*

[81] Senkov, O. N., Senkova, S. V., Miracle, D. B. & Woodward, C. Mechanical properties of low- density, refractory multi-principal element alloys of the Cr-Nb-Ti-V-Zr system. *Mater. Sci. Eng. A565,51–62 (2013)*

[82] Wu, Y.D; Cai, Y.H; Wang, T; Si, J.J; Zhu, J; Wang, Y.D; Hui, X.D. A refractory Hf25Nb25Ti25Zr25 high-entropy alloy with excellent structural stability and tensile properties. *Mater. Lett.130,277–280 (2014)*

[83] S.T. Chen, W.Y. Tang, Y.F. Kuo, S.Y. Chen, C.H. Tsau, T.T. Shun, J.W. Yeh. Microstructure and properties of age-hardenable $Al_xCrFe_{1.5}MnNi_{0.5}$ alloys. *Mater. Sci. Eng. A, 527 (2010), pp. 5818–5825*

[84] C. Juan, C. Hsu, C. Tsai, W. Wang, T. Sheu, J. Yeh, S. Chen. On microstructure and mechanical performance of $AlCoCrFeMo_{0.5}Ni_x$ high-entropy alloys. *Intermetallics, 32 (2013), pp. 401–407*

[85] B. Gludovatz, A. Hohenwarter, D. Catoor, E.H. Chang, E.P. George, R.O. Ritchie. A fracture-resistant high-entropy alloy for cryogenic applications. *Science, 345 (2014), pp. 1153–1158*

[86] M.J. Yao, K.G. Pradeep, C.C. Tasan, D. Raabe. A novel, single phase, non-equiatomic FeMnNiCoCr high-entropy alloy with exceptional phase stability and tensile ductility. *Scr. Mater, 72–73 (2014), pp. 5–8*

[87] J.W. Qiao, S.G. Ma, E.W. Huang, C.P. Chuang, P.K. Liaw, Y. Zhang. Microstructural characteristics and mechanical behaviors of AlCoCrFeNi high-entropy alloys at ambient and cryogenic temperatures. *Mater. Sci. Forum, 419 (2011), pp. 419–425*

[88] M.H. Tsai, J.W. Yeh, J.Y. Gan. Diffusion barrier properties of AlMoNbSiTaTiVZr high-entropy alloy layer between copper and silicon. *Thin Solid Films, 516 (2008), pp. 5527–5530*

[89] T. Zuo, X. Yang, P. Liaw, Y. Zhang. Influence of Bridgman solidification on microstructures and magnetic behaviors of a non-equiatomic FeCoNiAlSi high-entropy alloy. *Intermetallics Vol 67 (2015)*

[90] N. Zhi-sheng, Z. Jing-chuan, Y. Hai-ling, L. Zhong-hong. First principles calculation of intermetallic compounds in FeTiCoNiVCrMnCuAl system high entropy alloy. *ScienceDirect (2012)*

[91] PENG J Z, WANG Y F, GRAY M F. First-principles study of structural stabilities and electronic properties of MgNd intermetallic compounds [J]. *Physica B, 2008, 403: 2344-2348*

[92] LIN L, LIANG P, YANG L, CHEN L J, LIU Z, WANG Y M. Phase stability comparison by first principle calculation and experimental observation of microstructure evolution in a Mg6Gd2Zn (wt%) alloy [J]. *Mat Sci Eng A, 2010, 527: 2643-2648*

[93] M. Troparevsky, J. Morris, P. Kent,A. Lupini, G. Stocks. Criteria for Predicting the Formation of Single-Phase High-Entropy Alloys. *Physical Review (2015)*

[94] J. Li, W. Jia, J. Wang, H. Kou, D. Zhang, E. Beaugnon. Enhanced mechanical properties of a CoCrFeNi high entropy alloy by supercooling method. *Materials and Design. Jan 2016.*

[95] W.R. Wang, W.L. Wang, J.W. Yeh. Phases, microstructure and mechanical properties of Al_xCoCrFeNi high-entropy alloys at elevated temperatures. *J. Alloys Compd., 589 (2014), pp. 143–152*

[96] T. Egami, W. Guo, P.D. Rack, T. Nagase. Irradiation resistance of multicomponent alloys. *Metall. Mater. Trans. A, 45 (2013), pp. 180–183*

[97] Z. Hu, Y. Zhan, G. Zhang, J. She, C. Li. Effect of rare earth Y addition on the microstructure and mechanical properties of high entropy AlCoCrCuNiTi alloys. *Mater. Des., 31 (2010), pp. 1599–1602*

[98] J. Chen, P.Y. Niu, Y.Z. Liu, Y.K. Lu, X.H. Wang, Y.L. Peng, J.N. Liu. Effect of Zr content on microstructure and mechanical properties of AlCoCrFeNi high entropy alloy.

[99] Y. Dong, L. Jiang, H. Jiang, Y.P. Lu, T.M. Wang, T.J. Li. Effects of annealing treatment on microstructure and hardness of bulk $AlCrFeNiMo_{0.2}$ eutectic high-entropy alloy. M*ater. Des., 82 (2015), pp. 91–97*

[100] L.C. Tsao, C.S. Chen, C.P. Chu. Age hardening reaction of the $Al_{0.3}CrFe_{1.5}MnNi_{0.5}$ high entropy alloy. *Mater. Des., 36 (2012), pp. 854–858.*

[101] T.T. Shun, L.Y. Chang, M.H. Shiu. Age-hardening of the $CoCrFeNiMo_{0.85}$ high-entropy alloy. *Mater. Charact., 81 (2013), pp. 92–96*

[102] Free energy changes in reactions. (Accessed March 2016). Retrieved from *http://chem.libretexts.org/Core/Physical_Chemistry/Thermodynamics/Introduction_to_Thermodynamics/Free_Energy_Changes_in_Reactions*

[103] Many-body perspective versus Density Functional Theory. (Accessed January 2016). Retrieved from *http://www.magmat.org/wp-content/uploads/2014/04/DFT_vs_MB.png*

LIST OF APPENDICES

APPENDIX A: BINARY PHASE DIAGRAMS

Phase diagrams from the National Physical Laboratory of the United Kingdom using MTDATA softwar

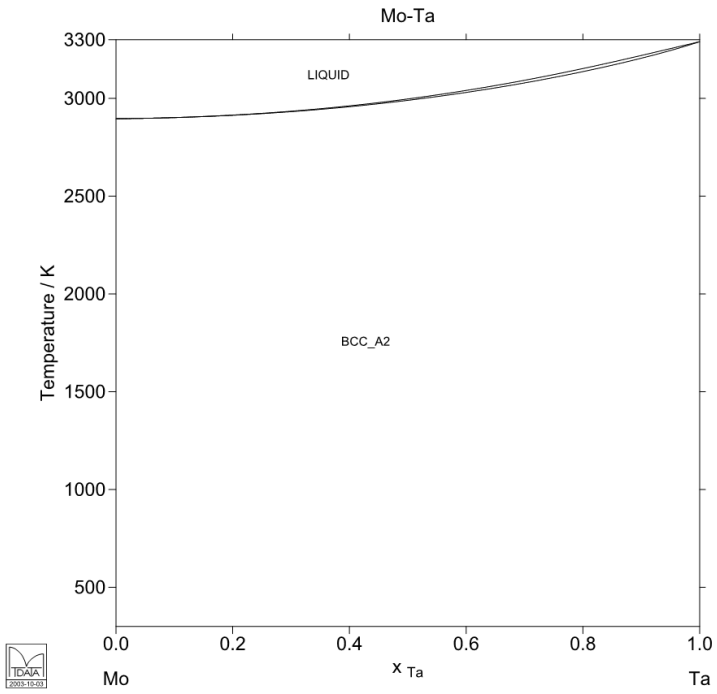
Mo-Ta
LIQUID
BCC_A2
Temperature / K
3300
3000
2500
2000
1500
1000
500
0.0
0.2
0.4
0.6
0.8
1.0
x Ta
Mo
Ta

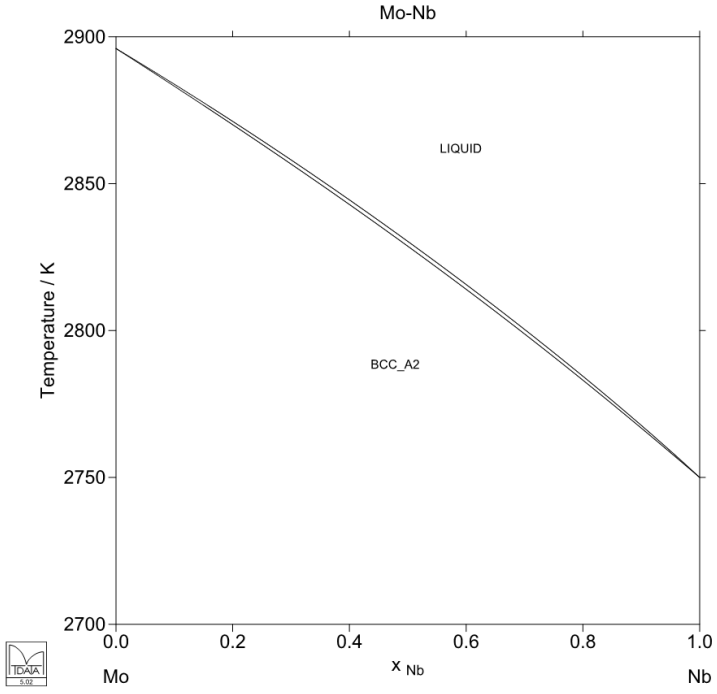
Mo-Nb
LIQUID
BCC_A2
Temperature / K
2900
2850
2800
2750
2700
0.0
0.2
0.4
0.6
0.8
1.0
x Nb
Mo
Nb

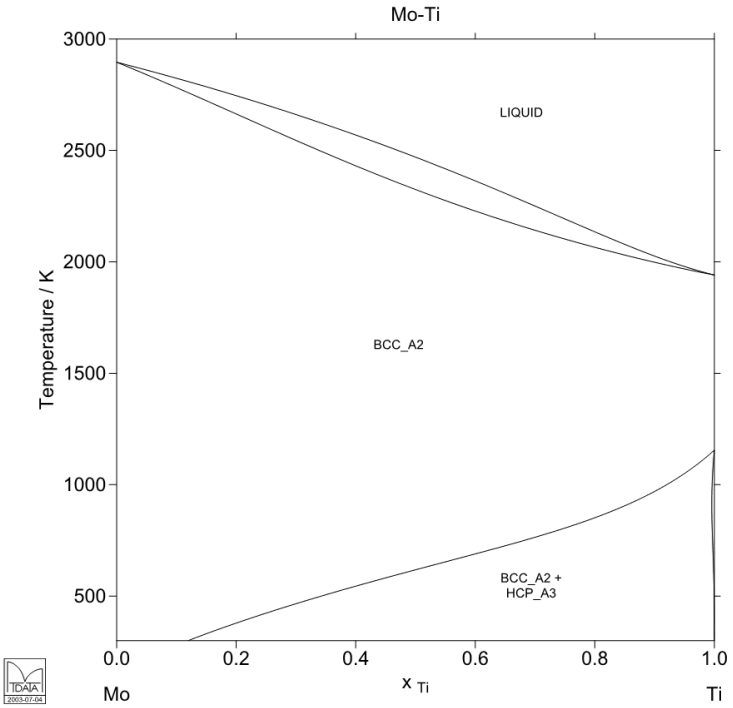
Mo-Ti
3000
2500
2000
1500
1000
500
Temperature / K
LIQUID
BCC_A2
BCC_A2 +
HCP_A3
0.0
0.2
0.4
0.6
0.8
1.0
x Ti
Mo
Ti
TDAIA
2003-07-04

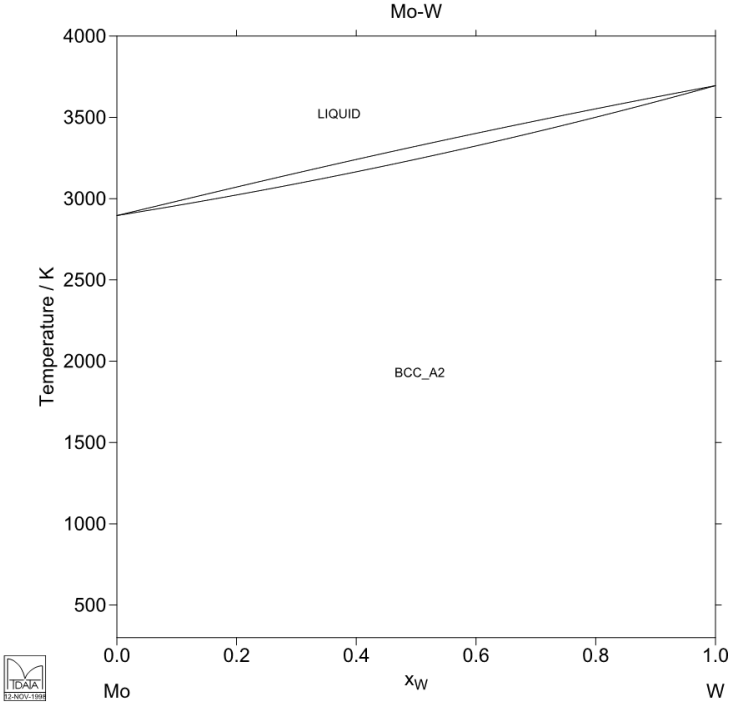
Mo-W
4000
3500
3000
2500
2000
1500
1000
500
Temperature / K
LIQUID
BCC_A2
0.0
0.2
0.4
0.6
0.8
1.0
xW
Mo
W
TDAIA
12-NOV-1999

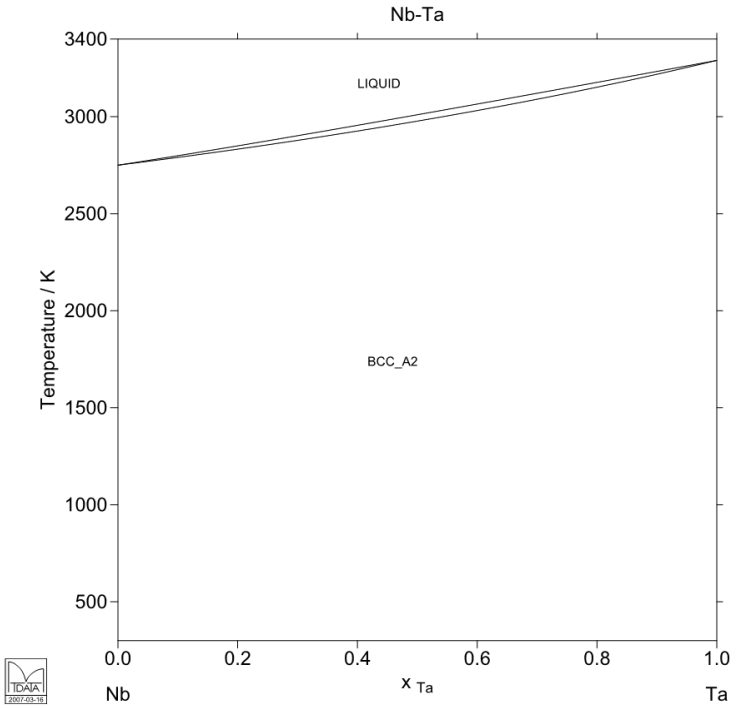
Nb-Ta
3400
3000
2500
2000
1500
1000
500
Temperature / K
LIQUID
BCC_A2
0.0
0.2
0.4
0.6
0.8
1.0
x Ta
Nb
Ta
TDATA
2007-03-16

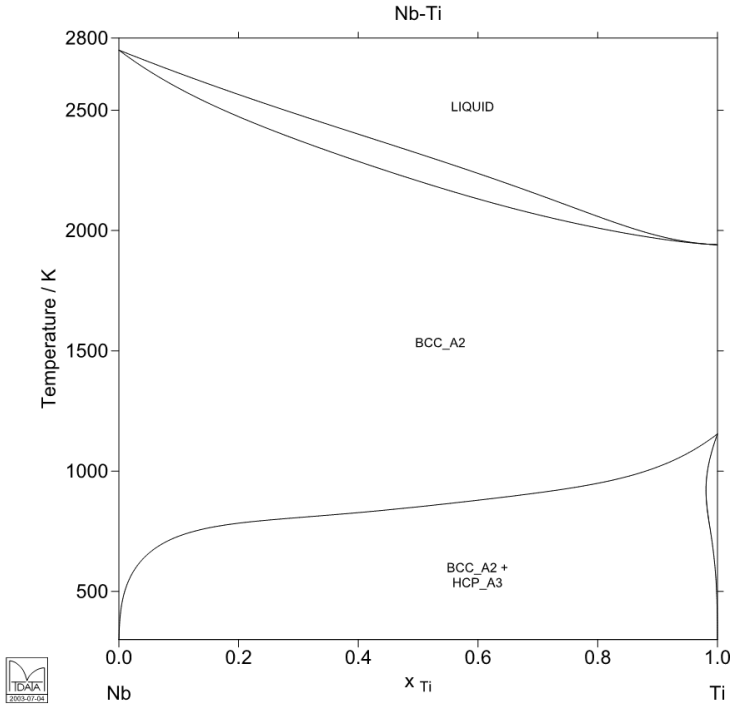
Nb-Ti
2800
2500
2000
1500
1000
500
Temperature / K
LIQUID
BCC_A2
BCC_A2 +
HCP_A3
0.0
0.2
0.4
0.6
0.8
1.0
x Ti
Nb
Ti
TDATA
2003-07-04

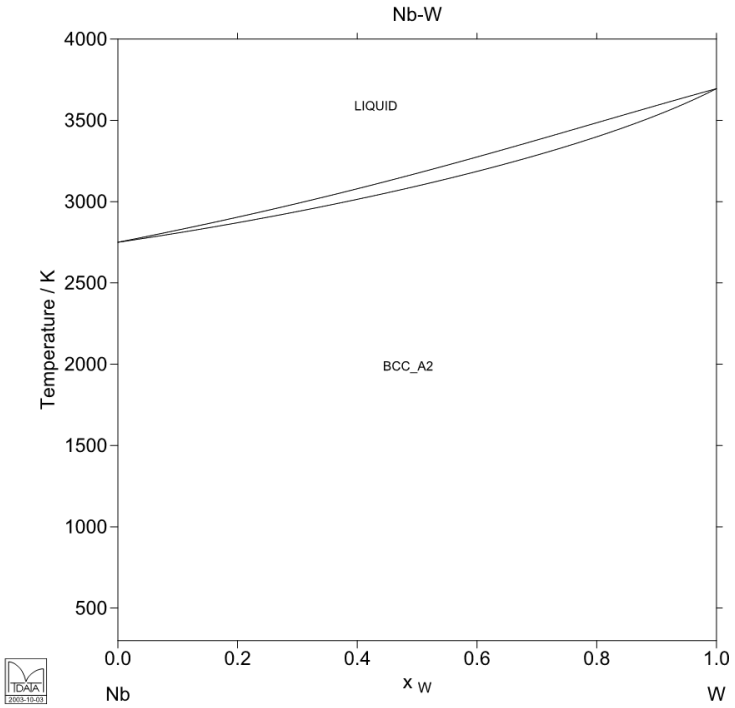
Nb-W
4000
3500
3000
2500
2000
1500
1000
500
Temperature / K
LIQUID
BCC_A2
0.0
0.2
0.4
0.6
0.8
1.0
x W
Nb
W
TDATA
2003-10-03

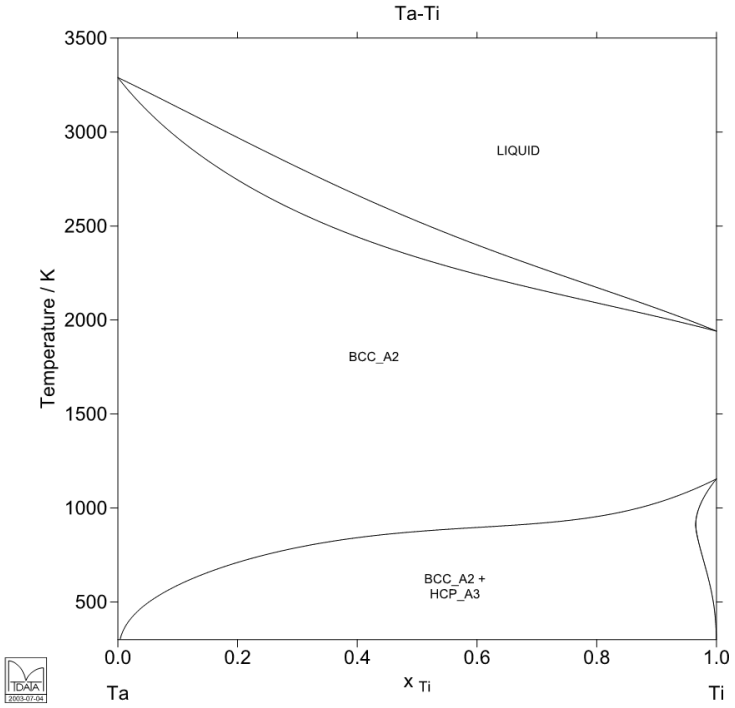
Ta-Ti
3500
3000
2500
2000
1500
1000
500
Temperature / K
LIQUID
BCC_A2
BCC_A2 +
HCP_A3
0.0
0.2
0.4
0.6
0.8
1.0
x Ti
Ta
Ti
TDATA
2003-07-04

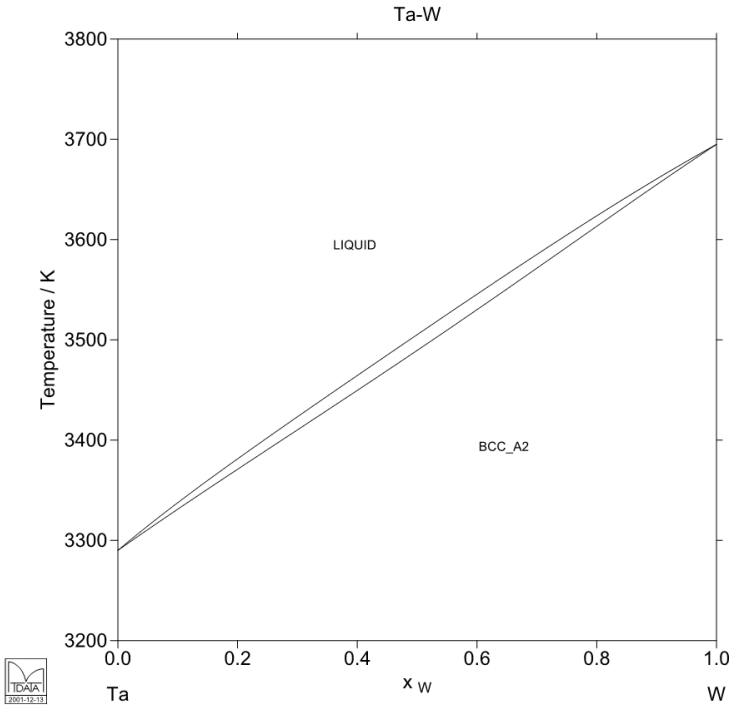
Ta-W
3800
3700
3600
3500
3400
3300
3200
Temperature / K
LIQUID
BCC_A2
0.0
0.2
0.4
0.6
0.8
1.0
x W
Ta
W
TDATA
2001-12-13

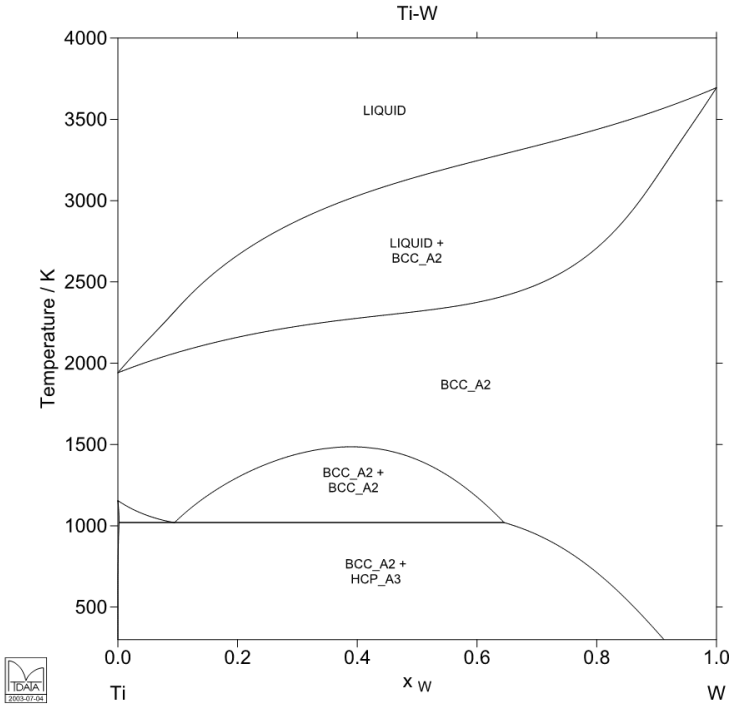
Ti-W
4000
3500
3000
2500
2000
1500
1000
500
Temperature / K
LIQUID
LIQUID +
BCC_A2
BCC_A2
BCC_A2 +
BCC_A2
BCC_A2 +
HCP_A3
0.0
0.2
0.4
0.6
0.8
1.0
x W
Ti
W
TDATA
2003-07-04

APPENDIX B: CASTEP OUTPUT FOR ELASTIC CONSTANT CALCULATI

```
 ================================================
 Elastic constants from Materials Studio: CASTEP
 ================================================

        Summary of the calculated stresses
        **********************************

 Strain pattern:      1
 =====================

 Current amplitude: 1
 Transformed stress tensor (GPa) :
      -5.467343        0.018397       -0.032430
       0.018397       -6.130111       -0.005994
      -0.032430       -0.005994       -6.161061

 Current amplitude: 2
 Transformed stress tensor (GPa) :
      -6.218680        0.006892       -0.022580
       0.006892       -6.428543       -0.006009
      -0.022580       -0.006009       -6.451257

 Current amplitude: 3
 Transformed stress tensor (GPa) :
      -6.961587        0.001914       -0.014420
       0.001914       -6.729766        0.001667
      -0.014420        0.001667       -6.727032

 Current amplitude: 4
 Transformed stress tensor (GPa) :
      -7.700028        0.009488       -0.020321
       0.009488       -7.026772        0.001134
      -0.020321        0.001134       -7.016600


  Stress corresponds to elastic coefficients (compact notation):
    1  7  8  9  10  11

  as induced by the strain components:
    1  1  1  1  1  1

     Stress    Cij       value of          value of
     index    index       stress            strain
       1        1        -5.467343         -0.003000
       1        1        -6.218680         -0.001000
       1        1        -6.961587          0.001000
       1        1        -7.700028          0.003000
C (gradient)     :     372.048100
Error on C       :       1.029106
Correlation coeff:       0.999992
Stress intercept :      -6.586910

       2        7        -6.130111         -0.003000
       2        7        -6.428543         -0.001000
       2        7        -6.729766          0.001000
       2        7        -7.026772          0.003000
C (gradient)     :     149.560300
Error on C       :       0.272212
Correlation coeff:       0.999997
Stress intercept :      -6.578798

       3        8        -6.161061         -0.003000
       3        8        -6.451257         -0.001000
       3        8        -6.727032          0.001000
```

```
       3        8        -7.016600          0.003000
C (gradient)     :     142.119600
Error on C       :       0.998750
Correlation coeff:       0.999951
Stress intercept :      -6.588988

       4        9        -0.005994         -0.003000
       4        9        -0.006009         -0.001000
       4        9         0.001667          0.001000
       4        9         0.001134          0.003000
C (gradient)     :      -1.453000
Error on C       :       0.563640
Correlation coeff:      -0.876736
Stress intercept :      -0.002301

       5        10        -0.032430         -0.003000
       5        10        -0.022580         -0.001000
       5        10        -0.014420          0.001000
       5        10        -0.020321          0.003000
C (gradient)     :      -2.224350
Error on C       :       1.319807
Correlation coeff:      -0.766038
Stress intercept :      -0.022438

       6        11         0.018397         -0.003000
       6        11         0.006892         -0.001000
       6        11         0.001914          0.001000
       6        11         0.009488          0.003000
C (gradient)     :       1.585250
Error on C       :       1.523295
Correlation coeff:       0.592689
Stress intercept :       0.009173

  Strain pattern:      2
  ======================

  Current amplitude: 1
  Transformed stress tensor (GPa) :
       -6.119646        0.020207       -0.019929
        0.020207       -5.456233        0.007309
       -0.019929        0.007309       -6.163398

  Current amplitude: 2
  Transformed stress tensor (GPa) :
       -6.435938        0.000701       -0.017868
        0.000701       -6.213279       -0.002323
       -0.017868       -0.002323       -6.443841

  Current amplitude: 3
  Transformed stress tensor (GPa) :
       -6.733824        0.001153       -0.009255
        0.001153       -6.952426        0.000238
       -0.009255        0.000238       -6.723114

  Current amplitude: 4
  Transformed stress tensor (GPa) :
       -7.030933        0.014492       -0.024496
        0.014492       -7.703742        0.000386
       -0.024496        0.000386       -7.004160


 Stress corresponds to elastic coefficients (compact notation):
   7  2  12  13  14  15
```

```
 as induced by the strain components:
   2  2  2  2  2  2

     Stress    Cij       value of          value of
     index    index       stress            strain
       1        7        -6.119646         -0.003000
       1        7        -6.435938         -0.001000
       1        7        -6.733824          0.001000
       1        7        -7.030933          0.003000
C (gradient)     :     151.587350
Error on C       :       1.639634
Correlation coeff:       0.999883
Stress intercept :      -6.580085

       2        2        -5.456233         -0.003000
       2        2        -6.213279         -0.001000
       2        2        -6.952426          0.001000
       2        2        -7.703742          0.003000
C (gradient)     :     374.083700
Error on C       :       1.155557
Correlation coeff:       0.999990
Stress intercept :      -6.581420

       3        12        -6.163398         -0.003000
       3        12        -6.443841         -0.001000
       3        12        -6.723114          0.001000
       3        12        -7.004160          0.003000
C (gradient)     :     140.077950
Error on C       :       0.114451
Correlation coeff:       0.999999
Stress intercept :      -6.583628

       4        13         0.007309         -0.003000
       4        13        -0.002323         -0.001000
       4        13         0.000238          0.001000
       4        13         0.000386          0.003000
C (gradient)     :       0.910400
Error on C       :       0.929770
Correlation coeff:       0.569248
Stress intercept :       0.001403

       5        14        -0.019929         -0.003000
       5        14        -0.017868         -0.001000
       5        14        -0.009255          0.001000
       5        14        -0.024496          0.003000
C (gradient)     :       0.254400
Error on C       :       1.739727
Correlation coeff:       0.102852
Stress intercept :      -0.017887

       6        15         0.020207         -0.003000
       6        15         0.000701         -0.001000
       6        15         0.001153          0.001000
       6        15         0.014492          0.003000
C (gradient)     :       0.834650
Error on C       :       2.608632
Correlation coeff:       0.220667
Stress intercept :       0.009138

  Strain pattern:      3
  ======================

  Current amplitude: 1
  Transformed stress tensor (GPa) :
```

```
      -6.155922        0.008359       -0.029844
       0.008359       -6.158643        0.005696
      -0.029844        0.005696       -5.462443

  Current amplitude: 2
  Transformed stress tensor (GPa) :
      -6.441608        0.005959       -0.021496
       0.005959       -6.439665        0.002034
      -0.021496        0.002034       -6.203567

  Current amplitude: 3
  Transformed stress tensor (GPa) :
      -6.729302        0.003643       -0.011261
       0.003643       -6.713845        0.000900
      -0.011261        0.000900       -6.958525

  Current amplitude: 4
  Transformed stress tensor (GPa) :
      -7.004302        0.012038       -0.026659
       0.012038       -6.988005        0.008787
      -0.026659        0.008787       -7.680630


 Stress corresponds to elastic coefficients (compact notation):
   8  12   3  16  17  18

 as induced by the strain components:
   3   3   3   3   3   3

    Stress    Cij       value of          value of
    index    index       stress            strain
      1        8        -6.155922         -0.003000
      1        8        -6.441608         -0.001000
      1        8        -6.729302          0.001000
      1        8        -7.004302          0.003000
C (gradient)     :     141.641700
Error on C       :       0.991906
Correlation coeff:       0.999951
Stress intercept :      -6.582783

      2        12        -6.158643         -0.003000
      2        12        -6.439665         -0.001000
      2        12        -6.713845          0.001000
      2        12        -6.988005          0.003000
C (gradient)     :     138.113300
Error on C       :       0.593691
Correlation coeff:       0.999982
Stress intercept :      -6.575039

      3        3         -5.462443         -0.003000
      3        3         -6.203567         -0.001000
      3        3         -6.958525          0.001000
      3        3         -7.680630          0.003000
C (gradient)     :     370.475950
Error on C       :       2.232792
Correlation coeff:       0.999964
Stress intercept :      -6.576291

      4        16          0.005696         -0.003000
      4        16          0.002034         -0.001000
      4        16          0.000900          0.001000
      4        16          0.008787          0.003000
C (gradient)     :      -0.406950
Error on C       :       0.941446
```

```
Correlation coeff:      -0.292305
Stress intercept :       0.004354

       5        17        -0.029844         -0.003000
       5        17        -0.021496         -0.001000
       5        17        -0.011261          0.001000
       5        17        -0.026659          0.003000
C (gradient)     :      -0.989500
Error on C       :       2.114448
Correlation coeff:      -0.314152
Stress intercept :      -0.022315

       6        18         0.008359         -0.003000
       6        18         0.005959         -0.001000
       6        18         0.003643          0.001000
       6        18         0.012038          0.003000
C (gradient)     :      -0.436050
Error on C       :       0.932465
Correlation coeff:      -0.313947
Stress intercept :       0.007500

  Strain pattern:      4
  ======================

  Current amplitude: 1
  Transformed stress tensor (GPa) :
       -6.585634       -0.008102       -0.014443
       -0.008102       -6.587926        0.098667
       -0.014443        0.098667       -6.572275

  Current amplitude: 2
  Transformed stress tensor (GPa) :
       -6.588410       -0.004301       -0.010711
       -0.004301       -6.579912        0.030487
       -0.010711        0.030487       -6.583260

  Current amplitude: 3
  Transformed stress tensor (GPa) :
       -6.578536        0.014211       -0.023118
        0.014211       -6.572776       -0.026066
       -0.023118       -0.026066       -6.588064

  Current amplitude: 4
  Transformed stress tensor (GPa) :
       -6.589304        0.025640       -0.030870
        0.025640       -6.590808       -0.086318
       -0.030870       -0.086318       -6.604982


 Stress corresponds to elastic coefficients (compact notation):
   9  13  16  4  19  20

 as induced by the strain components:
   4  4  4  4  4  4

     Stress    Cij       value of          value of
     index    index       stress            strain
       1        9        -6.585634         -0.003000
       1        9        -6.588410         -0.001000
       1        9        -6.578536          0.001000
       1        9        -6.589304          0.003000
C (gradient)     :       0.056800
Error on C       :       1.335907
Correlation coeff:       0.030051
```

```
Stress intercept :      -6.585471

       2        13        -6.587926         -0.003000
       2        13        -6.579912         -0.001000
       2        13        -6.572776          0.001000
       2        13        -6.590808          0.003000
C (gradient)     :       0.075500
Error on C       :       2.231024
Correlation coeff:       0.023922
Stress intercept :      -6.582856

       3        16        -6.572275         -0.003000
       3        16        -6.583260         -0.001000
       3        16        -6.588064          0.001000
       3        16        -6.604982          0.003000
C (gradient)     :       5.146250
Error on C       :       0.798991
Correlation coeff:       0.976733
Stress intercept :      -6.587145

       4        4          0.098667         -0.003000
       4        4          0.030487         -0.001000
       4        4         -0.026066          0.001000
       4        4         -0.086318          0.003000
C (gradient)     :      30.575400
Error on C       :       0.828517
Correlation coeff:       0.999267
Stress intercept :       0.004192

       5        19        -0.014443         -0.003000
       5        19        -0.010711         -0.001000
       5        19        -0.023118          0.001000
       5        19        -0.030870          0.003000
C (gradient)     :       3.084400
Error on C       :       1.168226
Correlation coeff:       0.881508
Stress intercept :      -0.019785

       6        20        -0.008102         -0.003000
       6        20        -0.004301         -0.001000
       6        20         0.014211          0.001000
       6        20         0.025640          0.003000
C (gradient)     :      -5.986900
Error on C       :       0.978462
Correlation coeff:      -0.974314
Stress intercept :       0.006862

  Strain pattern:      5
  ======================

  Current amplitude: 1
  Transformed stress tensor (GPa) :
       -6.584785        0.004635        0.057898
        0.004635       -6.579566        0.011284
        0.057898        0.011284       -6.605191

  Current amplitude: 2
  Transformed stress tensor (GPa) :
       -6.585937       -0.003398        0.007813
       -0.003398       -6.583983        0.001648
        0.007813        0.001648       -6.603759

  Current amplitude: 3
  Transformed stress tensor (GPa) :
```

```
       -6.583267        0.010714       -0.047597
        0.010714       -6.573703       -0.010068
       -0.047597       -0.010068       -6.573876

  Current amplitude: 4
  Transformed stress tensor (GPa) :
       -6.598905        0.008338       -0.112739
        0.008338       -6.588222       -0.014649
       -0.112739       -0.014649       -6.589429


 Stress corresponds to elastic coefficients (compact notation):
   10  14  17  19  5  21

 as induced by the strain components:
   5  5  5  5  5  5

     Stress    Cij       value of          value of
     index    index       stress            strain
       1        10        -6.584785         -0.003000
       1        10        -6.585937         -0.001000
       1        10        -6.583267          0.001000
       1        10        -6.598905          0.003000
C (gradient)     :       1.984500
Error on C       :       1.386974
Correlation coeff:       0.711220
Stress intercept :      -6.588223

       2        14        -6.579566         -0.003000
       2        14        -6.583983         -0.001000
       2        14        -6.573703          0.001000
       2        14        -6.588222          0.003000
C (gradient)     :       0.784400
Error on C       :       1.608643
Correlation coeff:       0.325964
Stress intercept :      -6.581369

       3        17        -6.605191         -0.003000
       3        17        -6.603759         -0.001000
       3        17        -6.573876          0.001000
       3        17        -6.589429          0.003000
C (gradient)     :      -3.858450
Error on C       :       2.937205
Correlation coeff:      -0.680576
Stress intercept :      -6.593064

       4        19         0.011284         -0.003000
       4        19         0.001648         -0.001000
       4        19        -0.010068          0.001000
       4        19        -0.014649          0.003000
C (gradient)     :       4.475750
Error on C       :       0.515608
Correlation coeff:       0.986987
Stress intercept :      -0.002946

       5        5         0.057898         -0.003000
       5        5         0.007813         -0.001000
       5        5        -0.047597          0.001000
       5        5        -0.112739          0.003000
C (gradient)     :      28.366050
Error on C       :       1.200514
Correlation coeff:       0.998214
Stress intercept :      -0.023656
```

```
       6        21         0.004635         -0.003000
       6        21        -0.003398         -0.001000
       6        21         0.010714          0.001000
       6        21         0.008338          0.003000
C (gradient)     :       -1.261050
Error on C       :        1.437236
Correlation coeff:       -0.527201
Stress intercept :        0.005072

  Strain pattern:      6
  ======================

  Current amplitude: 1
  Transformed stress tensor (GPa) :
       -6.591042         0.149072        -0.024860
        0.149072        -6.578065        -0.019223
       -0.024860        -0.019223        -6.585436

  Current amplitude: 2
  Transformed stress tensor (GPa) :
       -6.578535         0.042539        -0.020234
        0.042539        -6.578995        -0.011195
       -0.020234        -0.011195        -6.577483

  Current amplitude: 3
  Transformed stress tensor (GPa) :
       -6.589762        -0.037918        -0.013065
       -0.037918        -6.587541         0.011281
       -0.013065         0.011281        -6.594624

  Current amplitude: 4
  Transformed stress tensor (GPa) :
       -6.592020        -0.117747        -0.021494
       -0.117747        -6.583463         0.016717
       -0.021494         0.016717        -6.603030


 Stress corresponds to elastic coefficients (compact notation):
   11  15  18  20  21  6

 as induced by the strain components:
   6  6  6  6  6  6

     Stress    Cij       value of          value of
     index    index       stress            strain
       1        11         -6.591042         -0.003000
       1        11         -6.578535         -0.001000
       1        11         -6.589762          0.001000
       1        11         -6.592020          0.003000
C (gradient)     :       0.708050
Error on C       :       1.642982
Correlation coeff:       0.291497
Stress intercept :      -6.587840

       2        15         -6.578065         -0.003000
       2        15         -6.578995         -0.001000
       2        15         -6.587541          0.001000
       2        15         -6.583463          0.003000
C (gradient)     :       1.237000
Error on C       :       0.817816
Correlation coeff:       0.730456
Stress intercept :      -6.582016

       3        18         -6.585436         -0.003000
```

```
       3        18        -6.577483         -0.001000
       3        18        -6.594624          0.001000
       3        18        -6.603030          0.003000
C (gradient)     :       3.496150
Error on C       :       1.761564
Correlation coeff:       0.814396
Stress intercept :      -6.590143

       4        20        -0.019223         -0.003000
       4        20        -0.011195         -0.001000
       4        20         0.011281          0.001000
       4        20         0.016717          0.003000
C (gradient)     :      -6.514800
Error on C       :       1.131971
Correlation coeff:      -0.971111
Stress intercept :      -0.000605

       5        21        -0.024860         -0.003000
       5        21        -0.020234         -0.001000
       5        21        -0.013065          0.001000
       5        21        -0.021494          0.003000
C (gradient)     :      -0.863350
Error on C       :       1.215145
Correlation coeff:      -0.448924
Stress intercept :      -0.019913

       6        6          0.149072         -0.003000
       6        6          0.042539         -0.001000
       6        6         -0.037918          0.001000
       6        6         -0.117747          0.003000
C (gradient)     :      44.045700
Error on C       :       2.294863
Correlation coeff:       0.997296
Stress intercept :       0.008986


  ============================
  Summary of elastic constants
  ============================

 id  i  j       Cij (GPa)
 1   1  1     372.04810 +/-   1.029
 2   2  2     374.08370 +/-   1.156
 3   3  3     370.47595 +/-   2.233
 4   4  4      30.57540 +/-   0.829
 5   5  5      28.36605 +/-   1.201
 6   6  6      44.04570 +/-   2.295
 7   1  2     150.57382 +/-   0.831
 8   1  3     141.88065 +/-   0.704
 9   1  4      -0.69810 +/-   0.725
 10   1  5      -0.11993 +/-   0.957
 11   1  6       1.14665 +/-   1.120
 12   2  3     139.09563 +/-   0.302
 13   2  4       0.49295 +/-   1.209
 14   2  5       0.51940 +/-   1.185
 15   2  6       1.03582 +/-   1.367
 16   3  4       2.36965 +/-   0.617
 17   3  5      -2.42398 +/-   1.810
 18   3  6       1.53005 +/-   0.997
 19   4  5       3.78008 +/-   0.638
 20   4  6      -6.25085 +/-   0.748
 21   5  6      -1.06220 +/-   0.941

      ====================================
```

```
      Elastic Stiffness Constants Cij (GPa)
      =====================================

   372.04810   150.57382   141.88065    -0.69810    -0.11993     1.14665
   150.57382   374.08370   139.09563     0.49295     0.51940     1.03582
   141.88065   139.09563   370.47595     2.36965    -2.42398     1.53005
    -0.69810     0.49295     2.36965    30.57540     3.78008    -6.25085
    -0.11993     0.51940    -2.42398     3.78008    28.36605    -1.06220
     1.14665     1.03582     1.53005    -6.25085    -1.06220    44.04570

      ========================================
      Elastic Compliance Constants Sij (1/GPa)
      ========================================

   0.0034697  -0.0010484  -0.0009367   0.0001753  -0.0000699  -0.0000099
  -0.0010484   0.0034246  -0.0008851   0.0000020  -0.0001440  -0.0000257
  -0.0009367  -0.0008851   0.0033951  -0.0003356   0.0003429  -0.0001121
   0.0001753   0.0000020  -0.0003356   0.0342553  -0.0044145   0.0047620
  -0.0000699  -0.0001440   0.0003429  -0.0044145   0.0358820   0.0002321
  -0.0000099  -0.0000257  -0.0001121   0.0047620   0.0002321   0.0233899

Bulk modulus    =   219.83001 +/-  0.405 (GPa)

Compressibility =     0.00455 (1/GPa)

  Axis   Young Modulus        Poisson Ratios
         (GPa)
   X      288.21134       Exy=  0.3022 Exz=  0.2700
   Y      292.00716       Eyx=  0.3061 Eyz=  0.2585
   Z      294.54061       Ezx=  0.2759 Ezy=  0.2607

      ====================================================
      Elastic constants for polycrystalline material (GPa)
      ====================================================

                                Voigt       Reuss        Hill
Bulk modulus              :    219.96755   219.83001   219.89878
Shear modulus (Lame Mu)   :     66.26794    45.01532    55.64163
Lame lambda               :    175.78892   189.81980   182.80436

Universal anisotropy index:      2.36122
```

APPENDIX C: CASTEP OUTPUT FOR GEOMETRY OPTIMIZATION

```
                          ------------------------------
                                     Unit Cell
                          ------------------------------
        Real Lattice(A)                Reciprocal Lattice(1/A)
  6.5283804  -0.0256416   0.0078300        0.9624562   0.0033894  -0.0009906
 -0.0229930   6.5276865  -0.0049354        0.0037798   0.9625578   0.0007312
  0.0067267  -0.0049785   6.5188179       -0.0011532   0.0007247   0.9638552

                     Lattice parameters(A)       Cell Angles
                  a =    6.528436          alpha =   90.087285
                  b =    6.527729          beta  =   89.871987
                  c =    6.518823          gamma =   90.426908

               Current cell volume =  277.796520 A**3

                          ------------------------------
                                     Cell Contents
                          ------------------------------

            xxxxxxxxxxxxxxxxxxxxxxxxxxxxxxxxxxxxxxxxxxxxxxxxxxxxxxxxxxxxxx
            x  Element    Atom        Fractional coordinates of atoms  x
            x            Number          u          v          w      x
            x-----------------------------------------------------------x
            x  Nb           1         0.001195   0.000962   0.001208   x
            x  Nb           2         0.254655   0.256781   0.254909   x
            x  Nb           3         0.498341   0.498921  -0.010008   x
            x  Nb           4         0.744668   0.742720   0.254902   x
            x  Mo           1         0.002392   0.496885   0.000062   x
            x  Mo           2         0.001851   0.002034   0.502089   x
            x  Mo           3         0.249371   0.253878   0.749326   x
            x  Mo           4         0.497635   0.497987   0.499169   x
            x  Ta           1         0.246212   0.750149   0.249946   x
            x  Ta           2         0.497591   0.002816   0.501382   x
            x  Ta           3         0.754617   0.249408   0.748759   x
            x  Ta           4         0.751087   0.747593   0.748503   x
            x  W            1         0.497558   0.002701  -0.000299   x
            x  W            2         0.754396   0.251126   0.249697   x
            x  W            3         0.003323   0.496832   0.501073   x
            x  W            4         0.245108   0.749207   0.749283   x
            xxxxxxxxxxxxxxxxxxxxxxxxxxxxxxxxxxxxxxxxxxxxxxxxxxxxxxxxxxxxxx


---------------------------------------------------------------------- <--
SCF
SCF loop      Energy           Fermi           Energy gain       Timer   <--
SCF
                               energy          per atom          (sec)   <--
SCF
---------------------------------------------------------------------- <--
SCF
Initial  -2.22389055E+004  0.00000000E+000                     1587.68  <--
SCF
      1  -2.22390131E+004  3.97580862E-001   6.72342498E-003    1590.04  <--
SCF
      2  -2.22390143E+004  3.97557807E-001   7.72642044E-005    1593.13  <--
SCF
      3  -2.22390076E+004  3.99353272E-001  -4.17578712E-004    1595.56  <--
SCF
      4  -2.22389931E+004  3.99542016E-001  -9.08019989E-004    1598.54  <--
SCF
      5  -2.22389919E+004  4.00004661E-001  -7.68296081E-005    1601.24  <--
SCF
      6  -2.22389917E+004  4.00087204E-001  -1.19221169E-005    1603.60  <--
SCF
```

```
      7  -2.22389917E+004  3.99998748E-001  -6.30249277E-007    1605.20  <--
SCF
      8  -2.22389917E+004  3.99995439E-001   4.43676849E-008    1606.62  <--
SCF
------------------------------------------------------------------------ <--
SCF

Final energy, E             =  -22238.92388734     eV
Final free energy (E-TS)    =  -22238.99166312     eV
(energies not corrected for finite basis set)

NB est. 0K energy (E-0.5TS)      =  -22238.95777523     eV


 ********************************** Forces
**********************************
 *
*
 *                        Cartesian components (eV/A)
*
 * ------------------------------------------------------------------------
*
 *                   x                    y                    z
*
 *
*
 * Nb        1     -0.01575              0.02857             -0.01349
*
 * Nb        2      0.02372             -0.04052              0.02921
*
 * Nb        3     -0.00196             -0.00799             -0.02401
*
 * Nb        4      0.00608              0.00430              0.03214
*
 * Mo        1     -0.00616             -0.00677             -0.00772
*
 * Mo        2      0.01701             -0.00323              0.03288
*
 * Mo        3     -0.02651             -0.00703             -0.00255
*
 * Mo        4      0.00503             -0.00828             -0.03813
*
 * Ta        1     -0.01163              0.01349             -0.00526
*
 * Ta        2     -0.00462              0.00413             -0.00027
*
 * Ta        3     -0.00140             -0.00573              0.01349
*
 * Ta        4      0.00834              0.03541              0.00251
*
 * W         1      0.00653              0.00538             -0.01314
*
 * W         2     -0.01729             -0.00121             -0.00363
*
 * W         3      0.00101             -0.00768              0.00053
*
 * W         4      0.01759             -0.00284             -0.00256
*
 *
*

*************************************************************************
*
```

```
 ***************** Stress Tensor *****************
 *                                                 *
 *          Cartesian components (GPa)             *
 * ----------------------------------------------- *
 *             x             y             z       *
 *                                                 *
 *  x      0.015934      0.003222      0.006451    *
 *  y      0.003222      0.024339     -0.017484    *
 *  z      0.006451     -0.017484     -0.001596    *
 *                                                 *
 *  Pressure:   -0.0129                            *
 *                                                 *
 ***************************************************

 +------------+-------------+-------------+-----------------+ <-- min BFGS
 |    Step    |   lambda    |   F.delta   |    enthalpy     | <-- min BFGS
 +------------+-------------+-------------+-----------------+ <-- min BFGS
 |  previous  |    0.000000 |    0.000022 |   -22238.984089 | <-- min BFGS
 | trial step |    1.000000 |  5.088E-006 |   -22238.983916 | <-- min BFGS
 +------------+-------------+-------------+-----------------+ <-- min BFGS

 BFGS: finished iteration    27 with enthalpy= -2.22389839E+004 eV

 +-----------+-----------------+-----------------+------------+-----+ <--
BFGS
 | Parameter |      value      |    tolerance    |    units   | OK? | <--
BFGS
 +-----------+-----------------+-----------------+------------+-----+ <--
BFGS
 |  dE/ion   |   1.079057E-005 |   2.000000E-005 |         eV | Yes | <--
BFGS
 |  |F|max   |   5.529954E-002 |   5.000000E-002 |       eV/A | No  | <--
BFGS
 |  |dR|max  |   1.766217E-003 |   2.000000E-003 |          A | Yes | <--
BFGS
 |   Smax    |   2.433852E-002 |   1.000000E-001 |        GPa | Yes | <--
BFGS
 +-----------+-----------------+-----------------+------------+-----+ <--
BFGS


================================================================================
===
 Starting BFGS iteration         28 ...
================================================================================
===

 +------------+-------------+-------------+-----------------+ <-- min BFGS
 |    Step    |   lambda    |   F.delta   |    enthalpy     | <-- min BFGS
 +------------+-------------+-------------+-----------------+ <-- min BFGS
 |  previous  |    0.000000 |  3.372E-006 |   -22238.983916 | <-- min BFGS
 +------------+-------------+-------------+-----------------+ <-- min BFGS


--------------------------------------------------------------------------------
---
 BFGS: starting iteration        28 with trial guess (lambda=  1.000000)
--------------------------------------------------------------------------------
```

VITA

Daniel Clark obtained his Bachelor of Business Administration from the University of Mississippi in 2009 and his Bachelor of Science in Mechanical Engineering from the University of Mississippi in 2013.

In 2014, he started working towards a Master of Science in Engineering Science with an emphasis in Mechanical Engineering at the University of Mississippi. He helped conduct research into sediment transport at the National Center for Physical Acoustics and worked with biologists at the National Center for Natural Products Research in order to extract oils from algae to convert to biofuel. He conducted his thesis research under the guidance of Dr. Amrita Mishra focusing on elastic properties of high entropy alloys.